253 (2025) 214005

Contents lists available at ScienceDirect

Geoenergy Science and Engineering

journal homepage: www.sciencedirect.com/journal/geoenergy-science-and-engineering

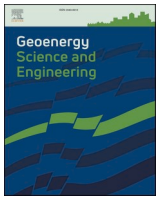

Experimental study on the impact of H_2S and H_2SO_4 in CO_2 on five different sealant compositions under conditions relevant for geological CO_2-storage

Reinier van Noort [a,*], Gaute Svenningsen [a], Kai Li [b,c]

[a] Institute for Energy Technology, Instituttveien 18, 2007, Kjeller, Norway
[b] Geoscience & Engineering Department, Delft University of Technology, the Netherlands
[c] Now at: Geothermal Energy & Reservoir Technology, Karlsruhe Institute of Technology, Karlsruhe, Germany

A B S T R A C T

The integrity of well sealants is a key challenge to secure geological storage of CO_2. While it has been well-established through experimental research that the exposure of such sealants to CO_2-bearing fluids can lead to carbonation, and potentially degradation during prolonged exposure or flow, the impact of impurities present in injected CO_2 has not received much consideration.

This paper reports exposure of five different sealants to simulated well conditions with supercritical CO_2 containing H_2S or H_2SO_4 as impurities. Three of these sealants are based on Portland Cement, while the other two are based on Calcium Aluminate Cement, and a rock-based geopolymer specifically developed for Geological CO_2 Storage (GCS). The impact of the impurities on these sealants was assessed through scanning electron microscopy with energy-dispersive X-ray spectroscopy, computed tomography scanning, and fluid chemical analysis, and compared to previous research where the same five sealants were exposed to clean CO_2 under otherwise identical conditions.

The results show that during exposure to CO_2-saturated water, the presence of H_2S mostly resulted in enhanced sealant alteration depths, and reduced carbonate precipitation. During exposure to wet supercritical CO_2, the presence of H_2S or H_2SO_4 resulted in reduced carbonate precipitation, and enhanced alteration depths in some (H_2S) or all (H_2SO_4) sealants. Additionally, relatively minor degradation was observed in the outer 100–200 μm of samples exposed in the presence of H_2SO_4. Overall, the impacts of impurities were more pronounced for sealants that were more affected by exposure to clean CO_2.

1. Introduction

CO_2 captured from a power plant or industrial process is likely to contain a range of additional components that are often referred to as impurities. While many impurities, such as N_2 or Ar, are chemically inert, some impurities may react and form products that potentially have deleterious effects on the transportation, injection and storage systems. While corrosion of steel pipes, tanks and other components is the key concern, potential reactions between the CO_2-stream and fluids, rocks and other solids in the storage reservoir also need to be considered.

Once an impure CO_2-stream is injected into a geological reservoir, the injected CO_2 will displace most of the pore fluid present in the reservoir (i.e., saline water or brine in case of injection into a saline aquifer), while also interacting with this fluid. CO_2 and certain impurities will dissolve into the reservoir fluid, and may react with other solutes present in this fluid. In return, components present in the reservoir (such as water, hydrocarbons, H_2S, etc.) may dissolve into the CO_2-phase. The partitioning of these various components between the water- and CO_2-phases will then lead to a chromatographic fractionation as components that preferentially partition into the water phase dissolve into pore water close to the injection zone, while components that prefer the CO_2-phase will concentrate at the leading edge of the migrating plume (Bachu and Bennion, 2009; Talman, 2015; Wolf et al., 2017; Xu et al., 2007). Consequently, components with much higher solubility in the water phase than in the CO_2 phase will accumulate in the hydrous reservoir pore fluid. Key impurities with higher affinity for water than CO_2 include reactive impurities such as SO_x, H_2S, and NH_3. These compounds are thus expected to accumulate in hydrous fluids near the injection point, for example in trapped pockets of water left within the CO_2-plume.

Within a CO_2-storage reservoir, the hydraulic sealants used as annular seals and plugs in the various wells provide some of the most reactive, and hence vulnerable materials. While the impact of CO_2-saturated water and wet supercritical CO_2 on wellbore cements has been investigated extensively in laboratory experiments (e.g., (Abid et al., 2015; Barlet-Gouédard et al., 2006; Bjørge et al., 2019; Chavez Panduro et al., 2017; Duguid, 2009; Duguid and Scherer, 2010; Gu et al., 2017; Jacquemet et al., 2012; Jacquemet et al., 2008; Kutchko et al., 2015;

This article is part of a special issue entitled: CCUS Geoenergy Frontiers published in Geoenergy Science and Engineering.

* Corresponding author.
E-mail address: Reinier@ife.no (R. van Noort).

https://doi.org/10.1016/j.geoen.2025.214005
Received 19 January 2025; Received in revised form 5 May 2025; Accepted 25 May 2025
Available online 28 May 2025
2949-8910/© 2025 The Author(s). Published by Elsevier B.V. This is an open access article under the CC BY license (http://creativecommons.org/licenses/by/4.0/).

Kutchko et al., 2007; Kutchko et al., 2011; Kutchko et al., 2009; Kutchko et al., 2008; Laudet et al., 2011; Lende et al., 2021; Lende et al., 2024; Lesti et al., 2013; Liteanu and Spiers, 2011; Matteo and Scherer, 2012; Omosebi et al., 2015; Sterpenich et al., 2014; Todorovic et al., 2020; Wigand et al., 2009; Zhang et al., 2014a; Zhang et al., 2014b; Zhang and Talman, 2014)), field samples (e.g., (Carey et al., 2007; Crow et al., 2009)), and numerical modelling (e.g., (Brunet et al., 2013; Hernández-Rodríguez et al., 2017; Jacquemet et al., 2012; Walsh et al., 2014; Xiao et al., 2017)), the impact of impurities within a CO_2-phase has not received as much attention. Most of that attention has been focused on H_2S, either by itself, or in combination with CO_2, as sealants may be exposed to H_2S in sour gas systems as well as in Geological CO_2 Storage (GCS) (cf. (Jacquemet et al., 2012; Jacquemet et al., 2008; Kutchko et al., 2011; Lende et al., 2021)). Experimental research addressing the potential impact of other impurities on cement integrity in a CO_2-storage reservoir appears to be lacking from the open literature.

While the maximum concentrations of impurities in published CO_2-specifications are very low (e.g., (Equinor, 2019; NorthernLights, 2024)), the preferential partitioning of key reactive impurities into the water phase can still lead to high concentrations of these impurities in the near-wellbore area. When further considering the mass of the cement seals compared to the mass of injected CO_2, the total quantities of injected impurities are very high. Thus, even low concentrations of impurities could potentially affect significant parts of the wellbore seals. It has been shown that common impurities, like H_2S, SO_2, NO_2 and O_2 may react and create nitric acid, sulphuric acid and elemental sulphur (Morland et al., 2019a,b). Considering these impurities and their reaction products, as well as the presence of water within the reservoir and seals, it is expected that SO_2 is the most deleterious single impurity, especially when this can react with water and a source of O_2 to form H_2SO_4 (Morland et al., 2022). Equilibrium calculations with thermodynamic software at pressure and temperature representative for storage reservoirs (80 °C and 10 MPa) show that even when H_2SO_4-concentrations in the CO_2 phase are very low (0-10 ppm-mol), most of the H_2SO_4 will partition to the hydrous phase, leading to severe acidification by up to 2 orders of magnitude (i.e., a decrease in pH by up to 2 units).

Therefore, the potential impact of impurities co-injected with CO_2 for storage in geological reservoirs on the cementitious materials used to seal wells remains a key knowledge gap in published research. To address this knowledge gap, we have performed experimental research exposing samples of five different sealant compositions to water and either clean CO_2 (van Noort et al., 2025), a CO_2-phase containing 1.6 mol% H_2S, or CO_2 in equilibrium with concentrated H_2SO_4. Next, the exposed samples as well as aqueous exposure solutions were analysed using a series of analysis techniques, including optical observations, sample mass measurements, Inductively Coupled Plasma Optical Emission Spectroscopy (ICP-OES), and Scanning Electron Microscopy (SEM) with Energy Dispersive X-ray Spectroscopy (EDS) to study how exposure affected the different materials. Then, the impacts of H_2S and H_2SO_4 as impurities in CO_2 on sealant integrity were assessed through comparison of the obtained results.

2. Materials and methods

2.1. Sealant compositions and samples

As part of the ACT-funded CEMENTEGRITY project, five different sealant compositions were extensively tested under conditions relevant for CO_2-injection and -storage (see Table 1). Three of these sealants (S1, S2 and S3) were based on Portland Cement (PC) with various additives, while one sealant (S4) was based on Calcium Aluminate Cement (CAC), and one sealant (S5) was a rock-based geopolymer being tailored for GCS-applications as part of the project. All samples used in this study were prepared by Halliburton in Norway, in accordance with API Recommended Practice 10B-2 (API, 2013), which included curing for 28 days at 150 °C and 30 MPa. After curing, the 12 mm diameter cylinders (still in the Teflon moulds) were cut to lengths of 30 mm and stored submerged in their curing water.

Table 1
Description of the different sealants that were studied.

Sealant	Description	Specific gravity
S1	Reference cement consisting of Class G cement plus 35 % BWOC[a] silica flour.	1.90
S2	Very low permeability composition based on Class G cement plus 35 % BWOC[a] silica flour, adding silica fume and MgO.	1.90
S3	Composition based on S2, replacing 28.5 % of the binder with RePlug™ (olivine-based CO_2-sequestering agent).	1.90
S4	CAC-based sealant composition.	1.80
S5	Geopolymer based on powdered granite with GGBFS[b] and micro-silica.	1.90

[a] By Weight of Cement.
[b] Ground Granulated Blast-Furnace Slag.

2.2. Sample exposure

Sample exposures were carried out in 400 ml titanium autoclaves. Titanium was used as material for the autoclaves because of its excellent chemical resistance under the selected conditions. For the H_2S tests, the autoclaves were half filled with water and half filled with H_2S-containing CO_2. For the H_2SO_4 tests, the autoclaves contained only CO_2 and a small quantity of acid. All exposure tests were carried out at 80 °C and 10 MPa.

The autoclaves had sample holders that allowed for the simultaneous exposure of multiple samples to either CO_2-saturated water (bottom), or wet supercritical CO_2 (top). The autoclaves were pressurised with CO_2 from a piston cylinder with nitrogen back-pressure. The test system and start-up/termination procedure have been described in a previous paper (van Noort et al., 2025). Demineralised water was used as the water phase, while the CO_2-phase was either pure CO_2 or CO_2 with 2.2 mol% H_2S (which resulted in 1.6 mol% H_2S in the CO_2 phase after equilibration with the water phase).

The CO_2-H_2S mixture was prepared directly in the piston cylinder using a high-precision balance. The required quantity of H_2S was first injected into the pressure-less piston cylinder (ambient pressure), followed by injection of high-pressure CO_2 using a booster pump, while accurately registering the mass added of both components. The exact H_2S concentration could then be calculated based on the measured masses of H_2S and CO_2 in the cylinder.

A different procedure was used to expose samples to CO_2 with H_2SO_4 (where H_2SO_4 was used as this represents the most chemically aggressive reaction product of SO_x). As the solubility of H_2SO_4 in CO_2 is very low (Morland et al., 2019a,b), practically all added H_2SO_4 (or SO_3) would quickly partition into the water-phase, where it would be significantly diluted and would only have a minor impact, if the same method to add H_2SO_4 was used as described above for H_2S. Furthermore, when using realistic H_2SO_4 concentrations in the CO_2-phase (for example 1-2 ppm-mol), the total quantity of H_2SO_4 in the system would be very small, and therefore rapidly depleted. Adding a significant quantity of H_2SO_4 to the water phase would likewise not be representative of how sealants might be exposed in a rising CO_2-plume. Thus, in an attempt to expose sealant samples directly to a supercritical CO_2-phase with realistically low H_2SO_4-concentration (saturation) while at the same time maintaining replenishment of any sulphuric acid that was consumed, the water phase was replaced by small vials with concentrated sulphuric acid (total 4–5 g of 96 wt.% sulphuric acid per experimental run). These vials with acid were placed on the lower shelf of the sample holder while the sealant samples were placed on the top shelf (about 10 cm distance between them). The sealant samples were water-saturated before exposure, but water was not added directly to the

system. The autoclaves were closed and then pressurised using pure CO_2, and exposures were otherwise carried out using the same procedures as the other tests. It was hypothesised that H_2SO_4 would dissolve from the vials into the CO_2-phase, and then partition into the pore fluid within the sealant samples, thus exposing these samples to a low concentration but buffered quantity of H_2SO_4 in CO_2. While pore water from the sealant samples would likewise dissolve in the CO_2 phase and then dissolve in the acid, some water would remain in the samples, adsorbed at gel surface and in narrow pores.

2.3. Chemical equilibrium calculations

Chemical equilibrium calculations were performed with the OLI-Studio software (v/12.0 and the MSE database with redox turned off), see Table 2. When pure water is equilibrated with clean CO_2, at 80 °C and 10 MPa, this leads to a hydrous liquid containing 1.5 mol% CO_2 (mostly as H_2CO_3) at a pH of 3.1, and a CO_2-phase that contains 1.0 mol % H_2O.

Addition of 2.2 mol% H_2S to the CO_2 phase (CO_2 feed) in this system then results in a hydrous liquid containing 1.5 mol% CO_2 (mostly as H_2CO_3) and 0.087 mol% H_2S (mostly as H_2S, with very minor HS^- and S^{2-} –equivalent to 1508 mg/kg total S in the hydrous phase), at a pH of 3.1. Upon equilibration, the CO_2-phase in this system then contains 1.0 mol% H_2O, and 1.6 mol% H_2S (less H_2S than in the CO_2 feed, as some H_2S partitioned to the water phase). Finally, when dry supercritical CO_2 is equilibrated with a small volume of concentrated sulphuric acid, this leads to a CO_2-phase containing 0.24×10^{-3} mol% H_2O and 0.091×10^{-3} mol% H_2SO_4 (mostly as H_2SO_4, but with traces of SO_3).

2.4. Analytical methods

Polished, resin-impregnated cross-sections of exposed and unexposed samples were photographed using a regular office scanning machine at 600 dpi. Next, these samples were investigated with SEM and EDS, using carbon coating to prevent charge-buildup. The SEM instrument was operated with 15 kV acceleration voltage. Most pictures were acquired using the backscatter electron detector, configured to maximise atomic number contrast. EDS maps (of elemental composition) were acquired using the AZtec v/6.1 software from Oxford Instruments. Each map was taken over a 800 μm × 550 μm area, with a 1024 x 704 pixels grid, giving a pixel density (resolution) of 0.8 μm × 0.8 μm (van Noort et al., 2025).

Fluids retrieved from the autoclaves after exposure were analysed by ICP-OES, on an Agilent 5800 ICP-OES, using the same methods as described previously (van Noort et al., 2025).

CT-scanning was performed on an X-ray micro-tomography (micro-CT) scanner (model CoreTOM, TESCAN), with a spatial resolution (voxel size) of about 13.5 μm. Panthera software (version 1.4, TESCAN) was then used to post-process the images, again using the same procedures as before (van Noort et al., 2025). CT-scanning was performed on the cut-off half cylinders, except for the S2 sample exposed to CO_2 with H_2SO_4. As this sample cracked during saw-cutting, a full sample was CT-scanned instead.

Table 2
Calculated equilibrium compositions of the hydrous liquids and CO_2-phases at 80 °C and 10 MPa.

	Water and CO_2 (mol%)	Water and CO_2 with H_2S (mol%)	CO_2 with H_2SO_4 (mol%)
Water in CO_2 phase	1.0	1.0	0.24×10^{-3}
H_2S in CO_2 phase	–	1.6	–
H_2SO_4 in CO_2 phase	–	–	0.091×10^{-3}
Total CO_2 in water	1.5	1.5	–
Total H_2S in water	–	0.087	–
pH	3.1	3.1	–

3. Results

The impact of exposure of cores of sealants S1-S5 to wet supercritical CO_2 and CO_2-saturated water, without impurities, was previously reported in (van Noort et al., 2025). The present work focuses on how the presence of H_2S (1.6 mol% in the CO_2-phase) and H_2SO_4 (vials of saturated solution placed in the autoclave, separate from the samples) affected these sealants.

3.1. Scanned sample cross-sections

Optical scans of the resin-impregnated sample cross-sections, shown in Fig. 1, display clear differences depending on exposure condition as well as sealant composition. In general, exposure to clean CO_2 and CO_2 with H_2SO_4 led to limited discolouration for sealants S2-S5 (Fig. 1b–e), while in sealant S1 (Fig. 1a) it caused a strong khaki-brownish discolouration. Exposure to CO_2 with H_2S led to more blue-grey, darker colours, which is assumed to be due to the differences in oxidation state between the different exposure conditions, as well as the formation of sulphide minerals in these samples. This could be ascertained through additional analyses, for example using XRD on powders recovered from exposed samples at different distances from the sample surface.

Here, it should also be noted that all S1 and S2 samples exposed to CO_2 in the presence of H_2SO_4 fractured during cross-sectioning. The three S1 samples cracked ahead of the sawcut, while the S2 samples not only cracked ahead of the sawcut, but also fractured parallel to the sample axis.

3.2. Mass and chemical changes

Fig. 2 shows relative sample mass changes as a function of exposure time, for all five sealants, and under all exposure conditions. Comparing the mass changes for S1 with and without H_2S shows that while the presence of H_2S had a negligible effect on mass changes due to direct exposure to wet supercritical CO_2, exposure to CO_2-saturated water with H_2S resulted in a lower increase in mass after 4 weeks, and a larger decrease after 16 weeks (leading to an overall decrease in mass by 4.6 % after 16 weeks while exposure to clean CO_2 led to an overall increase by 0.5 %). For sample S3, exposure to CO_2-saturated water with H_2S did not result in a decrease in mass at 16 weeks (relative to 4 or 8 weeks) as was observed for the sample exposed to CO_2-saturated water without H_2S. For the other samples, the impact of H_2S on mass changes due to exposure to CO_2-saturated water or wet supercritical CO_2 was negligible.

For the samples exposed to supercritical CO_2 in the presence of H_2SO_4, sample masses consistently decreased. This is most likely due to the removal of free water from these samples, as the CO_2 was not pre-saturated with water (to prevent dilution of the H_2SO_4 solution). It was hypothesised that the samples would maintain sufficient water in narrow (gel) pores, and adsorbed on surfaces to allow for chemical reactions requiring dissolution to proceed locally. To determine the initial water content of the sealants before exposure, sample cylinders of all five sealants were dried in an oven at 60 °C until stable mass was achieved (see Table 3).

3.3. Fluid chemical compositions

Fig. 3 shows plots of fluid composition, measured using ICP-OES, against time for the exposure water samples of the clean CO_2 and CO_2 with H_2S experiments. The composition at 0 weeks is the composition of the fluid the samples were cured, transported and stored in, and assumed equivalent to the initial pore fluid composition. For the experiments with H_2S, fluid samples were only taken after 16 weeks,

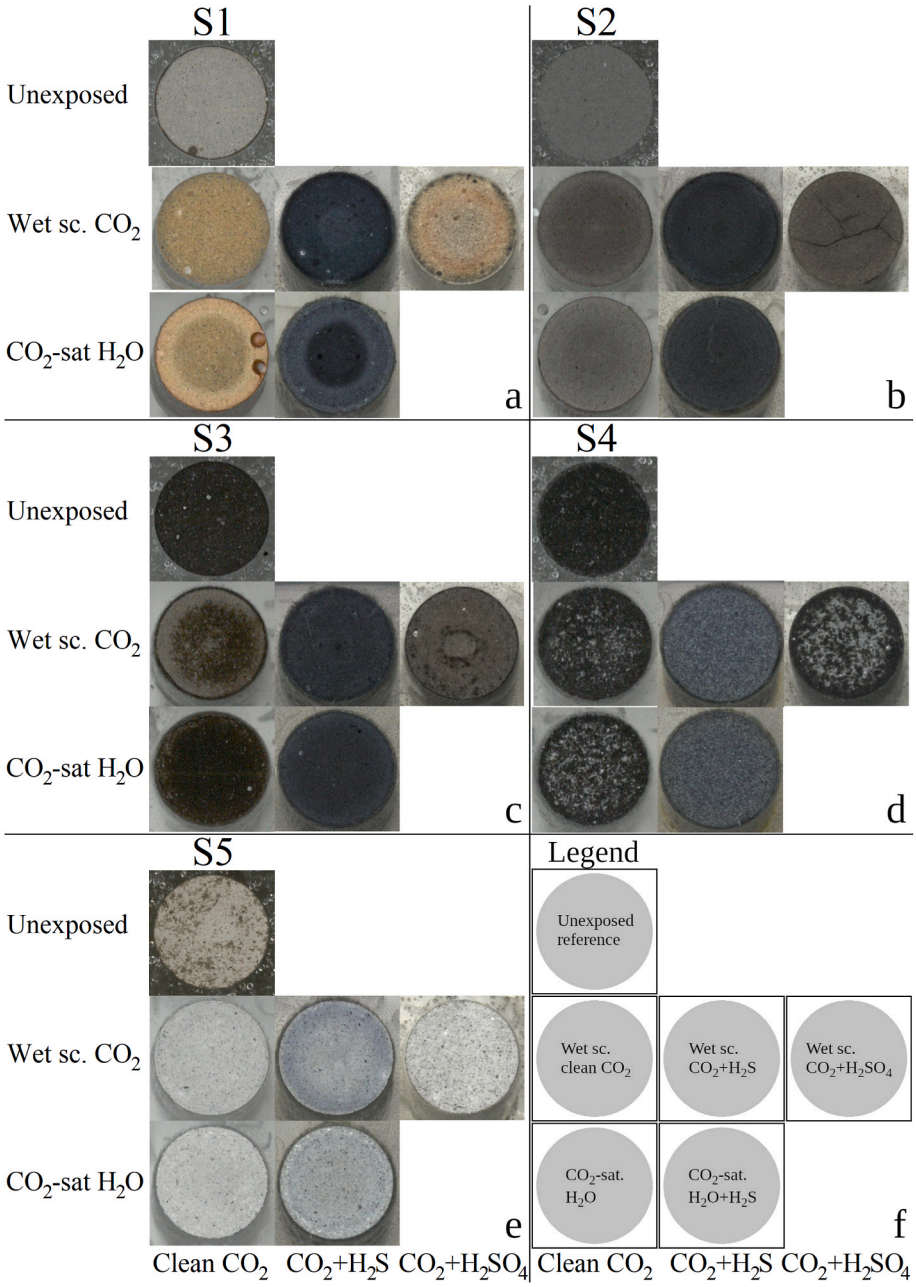

Fig. 1. Optical scans of resin-impregnated cross-sections of samples of S1 (a), S2 (b), S3 (c), S4 (d), and S5 (e), showing unexposed reference samples, as well as samples exposed for 16 weeks to CO_2-saturated water or directly to the supercritical CO_2 phase, using clean CO_2, CO_2 with 1.6 mol% H_2S, or CO_2 equilibrated with concentrated H_2SO_4. A legend mapping exposure conditions to optical scans is given in (f).

because of health and safety risks related to the toxicity of the H_2S. Comparing the fluid compositions after 16 weeks, most element contents in the fluids do not differ significantly in the presence of H_2S, though some key differences were observed. Firstly, while without H_2S the fluid Si-content for the S1 exposures was constant from 8 to 16 weeks at about 86–88 mg/kg, with H_2S, the fluid Si-content after 16 weeks was considerably higher at 458 mg/kg. Mg, K, and Ca contents were also elevated at 245 vs 71 mg/kg, 590 vs 65 mg/kg and 217 vs 131 mg/kg, respectively. For S2, fluid Na- and Mg-contents after 16 weeks exposure in the presence of H_2S were elevated at 161 vs 74 mg/kg and 494 vs 283 mg/kg, respectively. For S3, exposure in the presence of H_2S led to a considerably higher Mg-content in the fluid at 1646 vs 790 mg/kg, as well as relatively minor increases in Na- and K-contents. For S4, exposure in the presence of H_2S led to minor increases in fluid Mg- and Ca-contents. Finally, for S5, exposure to CO_2 with H_2S led to a lower Ca-content in the fluid, at 8 vs 35 mg/kg.

Interestingly, sulphur contents in the initial pore fluids are much higher than in the fluid samples taken after exposure. However, for sealants S1, S2 and S3, S-contents in the exposure fluids after exposure to CO_2 with H_2S are significantly higher than after exposure to clean CO_2 (263, 130 and 317 mg/kg vs. 84, 48 and 121 mg/kg, respectively). In contrast, S-contents of exposure fluids for sealants S4 and S5 are very low for both clean CO_2 (2.6 and < 0.01 mg/kg, respectively) and CO_2 with H_2S (19 and 7.0 mg/kg, respectively). Note that the equilibrium concentration of H_2S in water calculated for our experimental conditions, 0.087 mol%, equals ~1547 mg/kg S.

As in the H_2SO_4 experiments, samples were not directly exposed to the concentrated H_2SO_4, these liquids were not analysed. However, optical observations showed colour changes in many of the vials, to various levels of brown to near-black, indicating that the chemical

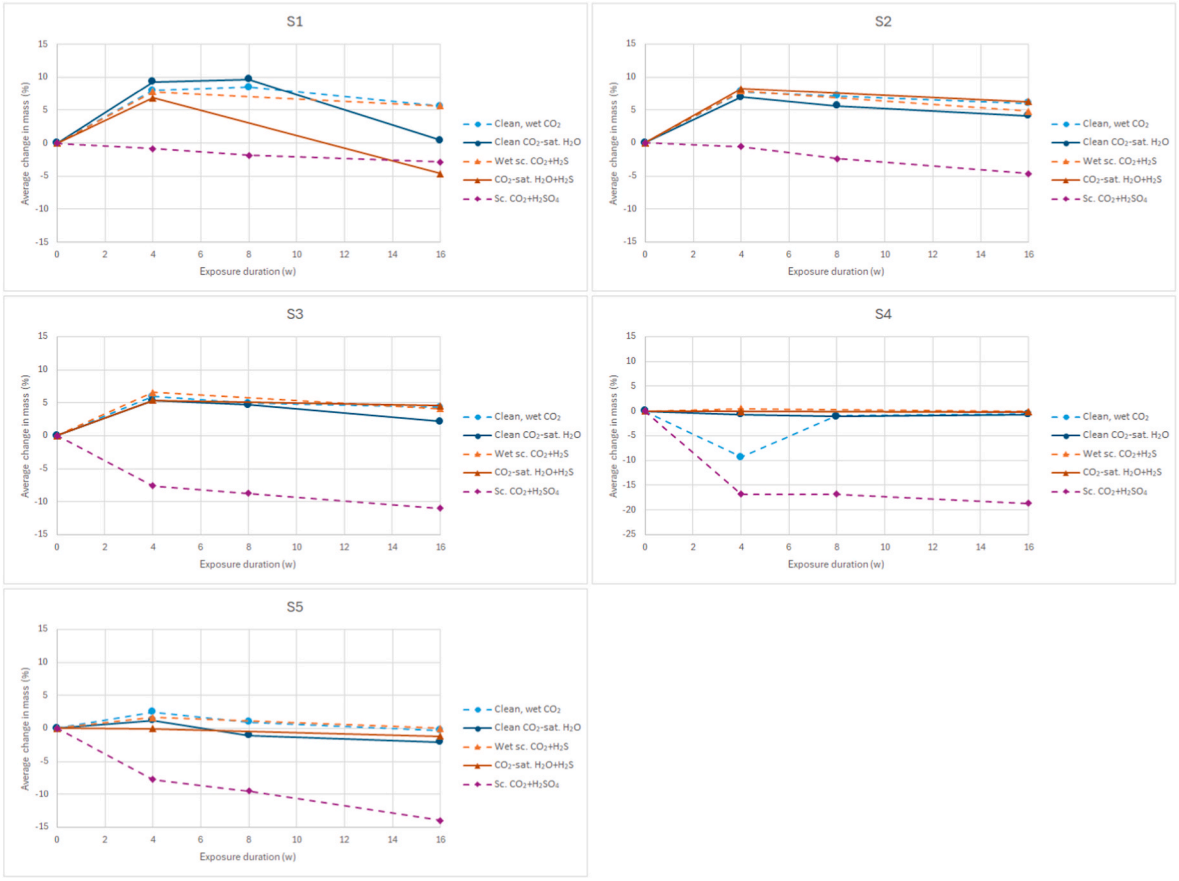

Fig. 2. Average changes in sample mass (mass %) relative to average initial sample mass (before exposure), plotted against exposure time for all five sealants, and under all exposure conditions. Relative sample mass changes of samples exposed to clean CO_2 were previously reported by (van Noort et al., 2025).

Table 3
Changes in sample mass upon drying at 60 °C. The wt.% of evaporable water is calculated as the total change in mass compared to the initial surface-dry, water-saturated mass.

Sealant	Surface-dry, water-saturated mass (g)	Dry mass (g)	Evaporable water (wt. %)
S1	6.184	4.756	23.1
S2	6.185	4.775	22.8
S3	6.157	4.641	24.6
S4	6.136	4.838	21.2
S5	6.140	4.760	22.5

compositions of these fluids did change.

3.4. Microstructural changes

Changes in sample microstructure were assessed based on SEM imaging with EDS mapping, as well as CT scans. Unfortunately, while the greyscale values in these CT scans are indicative of relative density, they are not absolute meaning individual scans cannot be compared to each other. As SEM and EDS analyses of the samples exposed to clean CO_2 already have been presented (van Noort et al., 2025), only the samples exposed to CO_2 with impurities will be presented here. When discussing changes in sample microstructure and composition, as seen in SEM micrographs with EDS mapping, ratios of key elements, such as the Ca/Si-ratio (or Ca/Al for S4), were used as indicators of chemical change. Ca is a mobile element here, while Si is expected to be more stationary. Likewise, the ratio of S/Si was used as indicator for penetration of sulphur into the exposed sealant samples. Element ratios, rather than element concentrations themselves, were used to eliminate variations in the analyses due to, for example, differences in porosity.

3.4.1. Sealant S1

CT scans of an unexposed sample of sealant S1, and samples exposed for 16 weeks are shown in Fig. 4. The larger dark and light spots visible in the unexposed reference sample (Fig. 4a) as well as some exposed samples are air bubbles (dark) that may be filled with carbonate (light). Irregular light particles are unreacted clinker particles. Comparison of the scans shows that exposure to CO_2-saturated water (with no H_2S – Fig. 4c) resulted in concentric reaction zones with (from inside to outside) a diffuse transition from normal to low density starting at about ~2000 μm from the sample surface, followed by an irregular transition to zone of elevated density between ~400 and ~1000 μm from the sample surface, and an outer zone of roughly ~110 μm wide with lowered density. The sample exposed to CO_2-saturated water with H_2S (Fig. 4e) shows a similar diffuse transition from unaffected density to a lower density starting at ~2600 μm from the sample surface, then a very irregular transition to areas with somewhat elevated density between ~600 and ~2000 μm. An outer zone with more reduced density was not observed.

In contrast, samples exposed to wet supercritical CO_2 show an elevated density in a thin zone (~240 μm) near the sample surface (Fig. 4b). The same trend was observed in the presence of H_2S (Fig. 4c). In the presence of H_2SO_4, the increase in density was more diffuse, and reached deeper into the sample. Furthermore, in the sample exposed to H_2SO_4, some inhomogeneity in density was observed in the outer ~100 μm (Fig. 4d).

Fig. 5 shows SEM cross-sections and element ratio curves of sealant S1 samples exposed to CO_2-saturated water, with the CO_2-phase containing 1.6 mol% H_2S, for 4 and 16 weeks. As can be seen in Fig. 5a, a 4-

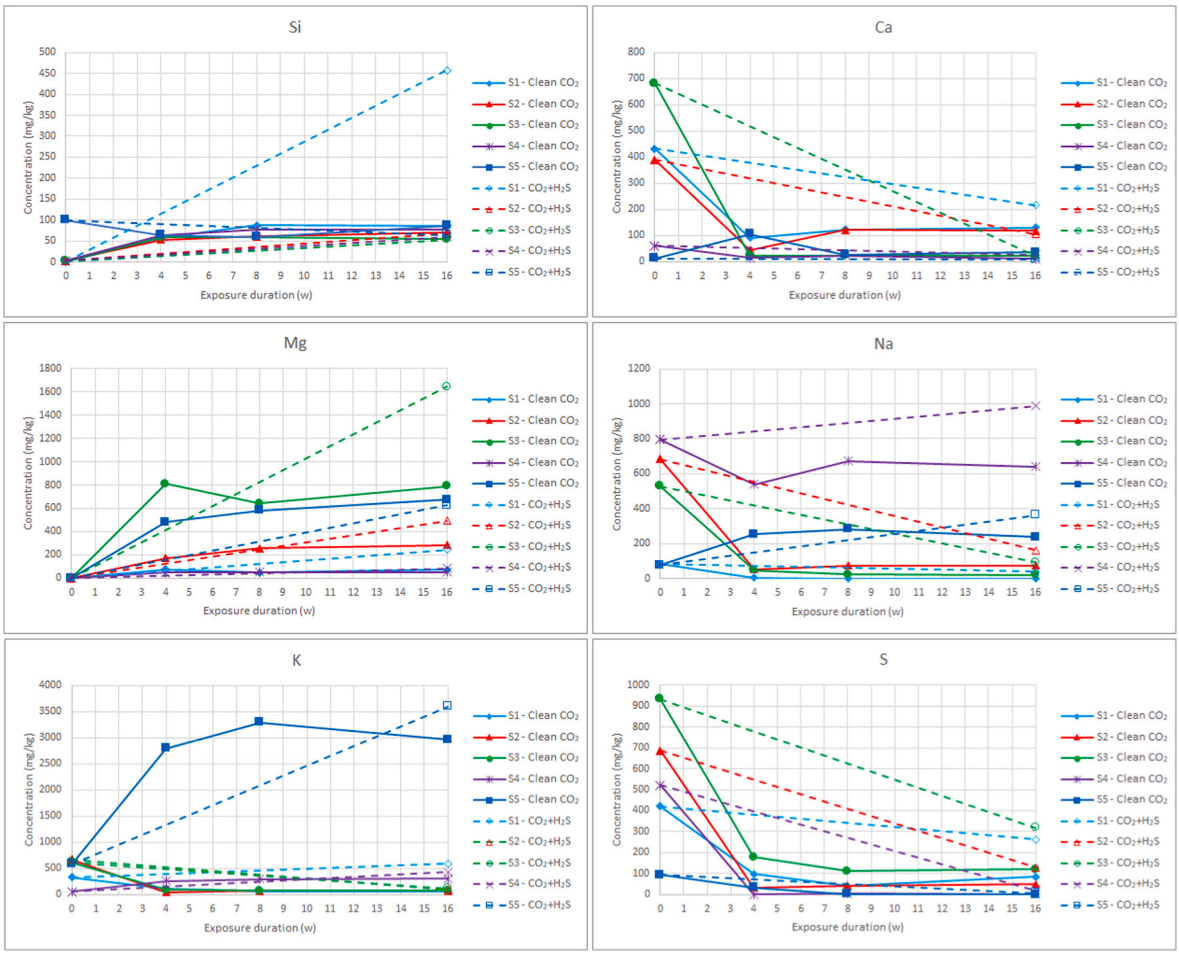

Fig. 3. Element concentrations in sampled fluids, measured using ICP-OES. Fluid compositions for the clean CO_2 exposures were previously reported by (van Noort et al., 2025).

week exposure to CO_2-saturated water led to an outer zone of up to ~80 μm thickness where dissolution and leaching led to a degradation of sample integrity. Inwards of that zone, a second zone was observed (700–800 μm wide), where the sample density was reduced while the integrity was mostly maintained. Within this zone, some localised areas of higher density were seen, representing more concentrated carbonate precipitation. Inwards of this zone, from ~900 to 1200 μm from the sample surface, the matrix porosity was somewhat reduced. Further inwards, the microstructure becomes relatively homogeneous and consistent to the sample core. The differences in microstructure correspond with a strong reduction of the Ca/Si-ratio in the outer 100 μm (somewhat increasing from the surface inwards), then a slight decrease in Ca/Si-ratio over the following ~140 μm to a minimum at about ~240 μm from the sample surface, and then a gradual increase to reference values, reached at about 900–1000 μm from the sample surface. S/Si-ratios are elevated throughout this sample compared to the reference value (0.076), but in particular in the outer ~150 μm, and somewhat less between about 150 and 500 μm from the surface.

In the sample exposed for 16 weeks, a strongly depleted outer zone where the integrity was degraded was similarly observed. A combination of increased porosity and carbonate precipitation was observed between 50 and 200 μm from the sample surface, while the Ca/Si-ratio was largely constant at considerably reduced values. Inwards of this zone, the Ca/Si-ratio dropped (to below 0.1), and the microstructure shows signs of being strongly depleted, leading to increased porosity and reduced gel density, though overall cohesion of the material was mostly maintained. Within this zone, the Ca/Si-ratio stays mostly constant to about ~1800 μm from the surface, though elevated Ca/ratios between ~300 and 900 μm from the surface correspond to areas of higher density due to Ca-carbonate precipitation. Ca/Si-ratios then increase gradually up to reference values at about 2900–3000 μm from the surface, while the microstructure changes gradually, becoming less porous as density and integrity increase, becoming relatively homogeneous and comparable to the sample centre at about ~2700 μm from the sample surface. As with the sample exposed for 4 weeks, S/Si-ratios are increased throughout the sample, though they are relatively low between 250 and 2700 μm, i.e., where Ca/Si-ratios are likewise depleted.

Very fine (mostly sub-micron) high-density (white) particles are observed in SEM images of both samples exposed to CO_2-saturated water with H_2S. Closer inspection of the sample exposed for 16 weeks shows that these particles are found throughout the sample. EDS analysis of a number of these particles indicated that they consist mainly Fe of and S, with about 1.5–2.0 S per Fe, though accurate quantitative analysis was prevented by the small particle size.

Fig. 6 shows sample cross-sections and element ratios for samples exposed directly to the H_2S-bearing CO_2-phase. After 4 weeks exposure, a thin outer precipitate layer was formed of a few μm thick. Inwards of this, the sample was partly dissolved, leading to a degradation of integrity and then gradually increasing integrity (decreasing porosity) inwards over ~150–200 μm. This is correlated to a minimum Ca/Si-ratio at the sample surface, gradually increasing to reference values 280–290 μm from the sample surface. Sample porosity is relatively reduced between 250 μm and ~700 μm from the sample surface. Inwards from there the sample microstructure appears relatively homogeneous through to the centre. The S/Si-ratio is elevated throughout the sample, but more so in the outer ~100–150 μm, indicating that H_2S fully

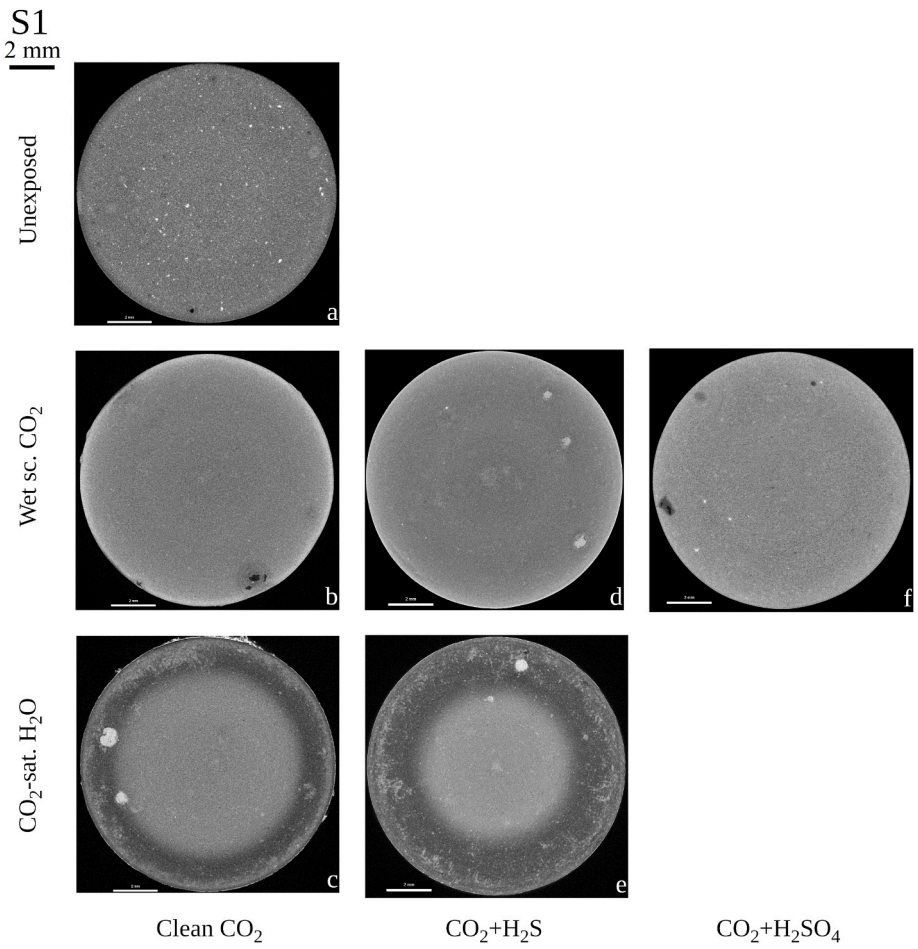

Fig. 4. CT-scans of sealant S1; a) unexposed, b) exposed to wet supercritical CO_2, c) exposed to CO_2-saturated water, d) exposed to wet supercritical CO_2 with 1.6 mol % H_2S, e) exposed to CO_2-saturated water with H_2S, and f) exposed to supercritical CO_2 equilibrated with concentrated H_2SO_4. The scalebars shown with the scans are 2 mm. All exposure durations were 16 weeks. CT scans of the unexposed reference sample and samples exposed to clean CO_2 taken from (van Noort et al., 2025).

penetrated the sample, but was also being bound in the outer part of the exposed sample.

In the sample exposed for 16 weeks, the outer zone contains relatively thick carbonate precipitates, though with some areas with higher porosity between the carbonates in the outer ~200 μm. Between ~200 and ~600 μm from the sample surface, this porosity is greatly reduced, while further inwards the microstructure looks quite homogeneous. The Ca/Si-ratio is somewhat elevated in the outer ~200 μm of the sample, decreasing gradually to reference values going inwards from the surface. The S/Si-ratio is elevated relatively constantly from surface to core, but somewhat more elevated in the outer ~400 μm. In these samples exposed to wet supercritical CO_2 with H_2S, very fine (sub-micron), high-density particles, similar to those identified as iron sulphides in the samples exposed to CO_2-saturated water, are likewise observed throughout the samples.

Fig. 7 shows samples exposed to supercritical CO_2 in the presence of H_2SO_4 for 4, 8 and 16 weeks. In all three samples, a thin (few μm thick) outer skin is observed, while inwards of that the sample has very high porosity, due to dissolution of material, with the sealant then gradually becoming more consistent moving inwards. In the sample exposed for 4 weeks, this degraded outer zone is ~150–200 μm wide and correlated to a depleted Ca/Si-ratio at the sample surface that increases moving inwards to reference values at ~150–200 μm. Between 200 and 800 μm from the surface, the sample has a relatively low porosity due to carbonate precipitation. From ~800 μm inwards, porosity increases gradually, until the sample becomes relatively homogeneous from ~1300 μm inwards. The S/Si-ratio is somewhat higher than reference values, and relatively constant from the surface inwards.

In the sample exposed for 8 weeks, similar zones are observed as described above. Here, the degraded outer zone is about 100–200 μm wide, and correlated to a depleted Ca/Si-ratio in the outer 100 μm only. Reduced porosities are observed down to ~900–1000 μm from the surface. S/Si-ratios are also somewhat elevated throughout the sample.

Finally, in the sample exposed for 16 weeks, degradation is observed in the outer ~100–200 μm, and correlated to a depleted Ca/Si-ratio in the outer ~80 μm, which then increases steeply to reference values between ~80 and 100 μm from the sample surface. Between ~200 μm and ~1000 μm from the sample surface, the porosity is relatively low, while from ~1000 μm inwards, the sample microstructure is relatively homogeneous. As with the other samples, S/Si-ratios are somewhat elevated, and constant throughout the sample.

3.4.2. *Sealant S2*

All CT scans of samples of sealant S2 are shown in Fig. 8. Similar to S1, exposure of S2 to CO_2-saturated water (Fig. 8c) led to concentric zones, with a relatively unaffected core surrounded by a lower density zone (~1020 μm wide), in turn bound by a zone with somewhat higher density than seen at the core (~800 μm wide), and a narrow outer zone of about 60 μm with reduced density. Here, the sample exposed to CO_2 containing H_2S (Fig. 8e) shows somewhat deeper penetration of these reaction zones, with enhanced density observed to about ~1040 μm from the sample surface, and subsequent depleted densities observed down to ~2030 μm from the sample surface. Exposure to supercritical CO_2 led to a minor increase in density in the outer zone of all samples,

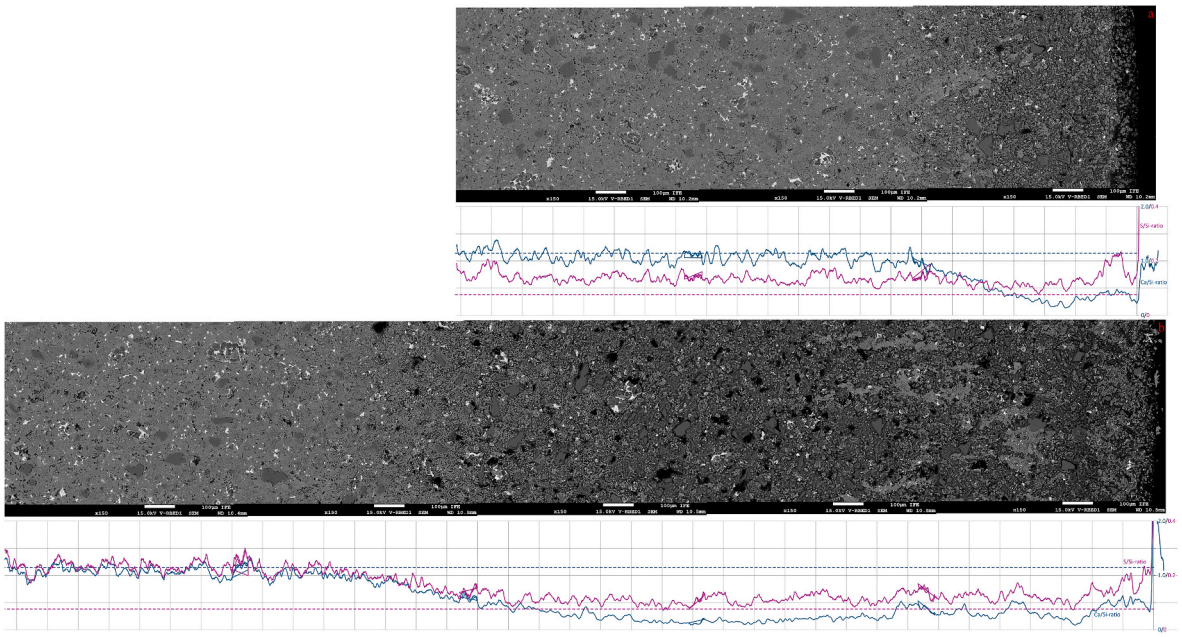

Fig. 5. SEM Micrographs of S1 samples exposed to water saturated with CO_2 containing 1.6 mol% H_2S for 4 (a) and 16 (b) weeks. The graphs underneath each micrograph show the Ca/Si (blue, on the 0–2.0 axis) and S/Si (purple, on the 0–0.4 axis) elemental ratios (atom %/atom %) measured along the micrograph using EDS. The dashed lines are reference values (average values) measured at the centre of an unexposed sample. Scalebars shown with the micrographs and gridline spacing for the graphs are 100 μm.

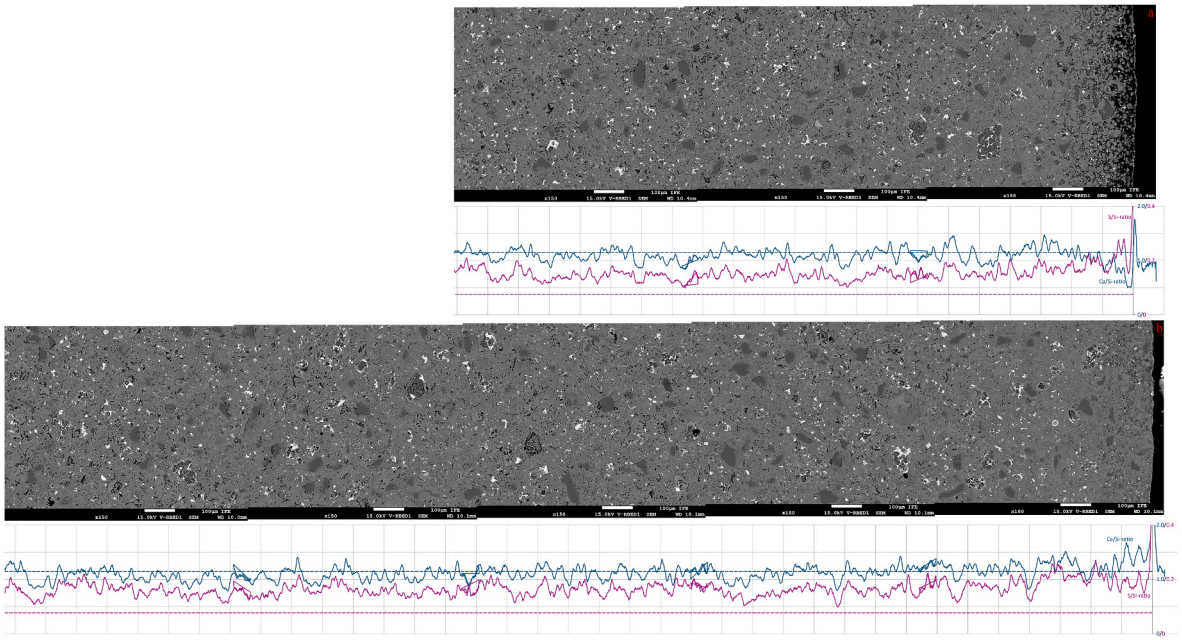

Fig. 6. SEM Micrographs of S1 samples exposed to wet supercritical CO_2 with 1.6 mol% H_2S for 4 (a) and 16 (b) weeks. The graphs underneath each micrograph show the Ca/Si (blue, on the 0–2.0 axis) and S/Si (purple, on the 0–0.4 axis) elemental ratios (atom %/atom %) measured along the micrograph using EDS. The dashed lines are reference values (average values) measured at the centre of an unexposed sample. Scalebars shown with the micrographs and gridline spacing for the graphs are 100 μm.

and compared to clean CO_2 (Fig. 8b) this alteration penetrated deeper into the sample in the presence of H_2S (Fig. 8d) and (to a lesser extent) H_2SO_4 (Fig. 8f).

Fig. 9 shows SEM cross-sections and element ratio curves of sealant S2 samples exposed to CO_2-saturated water, with the CO_2-phase containing 1.6 mol% H_2S, for 4 and 16 weeks. As can be seen in Fig. 9a, a 4-week exposure led to the formation of a thin (a few μm thick) precipitate layer on the outer surface of the exposed sample. Behind this precipitate layer, the material is partly dissolved and quite strongly degraded in a 10–20 μm wide zone, and then gradually increases in integrity. In the outer 200–400 μm of the sample, this correlates to a depleted Ca/Si-ratio, that increases gradually up to the reference value. Between ~400 and ~800 μm from the surface, the sample is somewhat less porous, indicating carbonate precipitation. Inwards from this, the sample is relatively homogeneous. On the surface of the sample exposed for 16 weeks, a similar thin precipitate layer is observed, behind which the

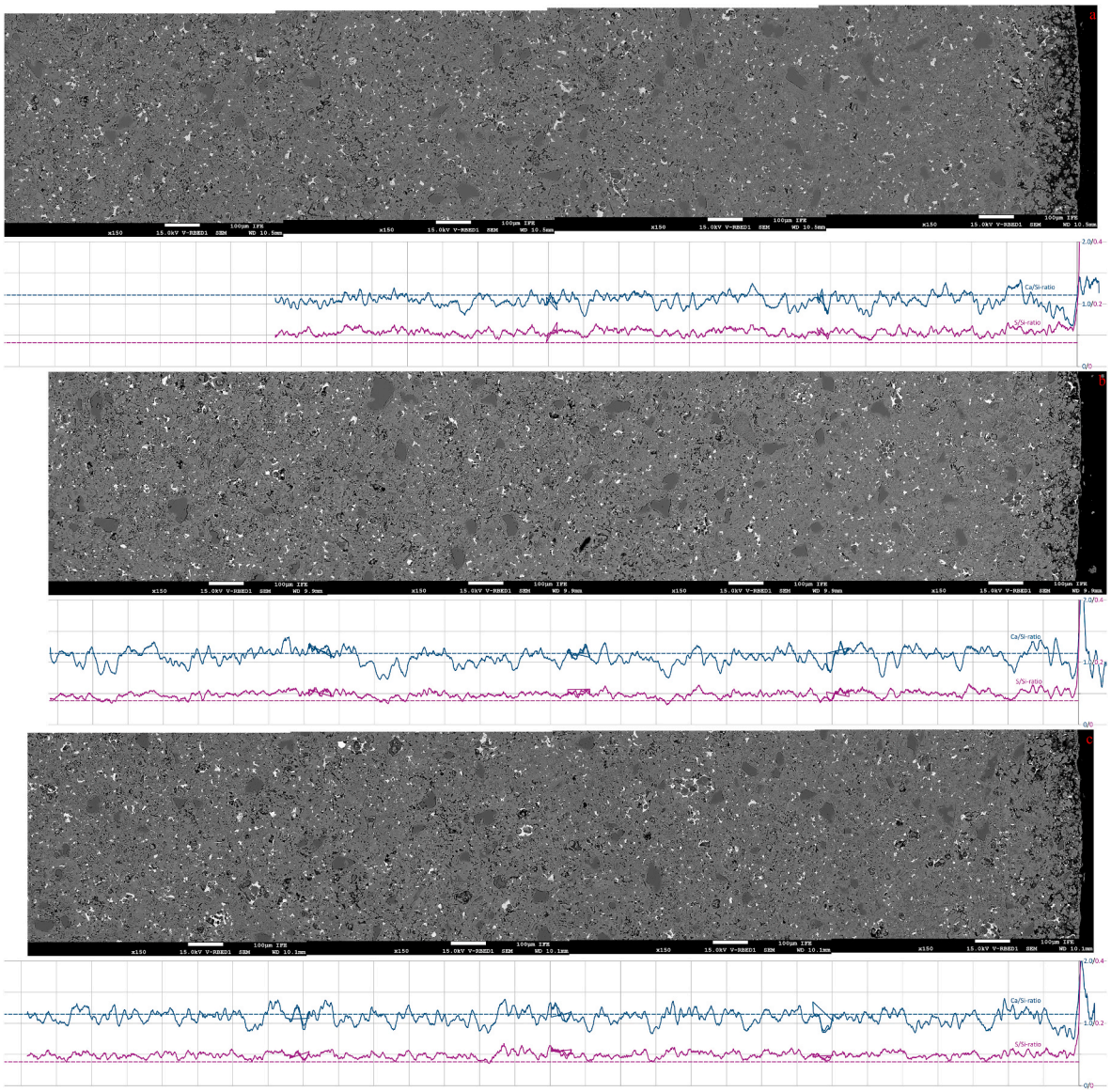

Fig. 7. SEM Micrographs of S1 samples exposed to wet supercritical CO_2 equilibrated with concentrated H_2SO_4 for 4 (a), 8 (b), and 16 (c) weeks. The graphs underneath each micrograph show the Ca/Si (blue, on the 0–2.0 axis) and S/Si (purple, on the 0–0.4 axis) elemental ratios (atom %/atom %) measured along the micrograph using EDS. The dashed lines are reference values (average values) measured at the centre of an unexposed sample. Scalebars shown with the micrographs and gridline spacing for the graphs are 100 μm.

sample is strongly degraded for ~100 μm. Inwards from that, over a ~150 μm wide zone, dense precipitation fills much of the porosity. This transitions abruptly into a zone with finer-grained precipitates and somewhat higher porosity. These microstructural zones are associated with a strongly depleted Ca/Si-ratio near the sample surface, that then increases inwards, reaching reference values at about 400–500 μm from the surface. Moving further inwards, the porosity increases again, and from ~700 μm from the surface the Ca/Si-ratio decreases below reference values. Between ~1100 μm and ~2100 μm from the surface, a zone of relatively high porosity is correlated with a depleted Ca/Si-ratio. Around ~2100 μm, this ratio increases to (near-)reference values, and then remains relatively constant, while the microstructure appears homogeneous from here. After both 4 and 16 weeks, the S/Si-ratio is elevated throughout the sample compared to the reference value (0.069), and relatively constant between surface and core. In these samples sub-micron high-density particles, similar to those identified as iron sulphides in the S1 samples exposed to CO_2-saturated water, are also observed. In the 4-week exposed sample, these are observed in the outer ~1500 μm, while in the 16-week exposed sample they were found throughout, though mostly in the outer ~1500 μm (and especially in the outer ~100 μm).

Fig. 10 shows sample cross-sections and element ratios for S2 samples exposed directly to the wet supercritical CO_2-phase, containing 1.6 mol% H_2S. The sample exposed for 4 weeks has a very thin precipitate layer on its outer surface, behind which the sample is somewhat degraded to ~20–30 μm from the sample surface, at which point a dense precipitate appears that fills up most pore space around silica particles. This dense precipitate is observed to about ~300 μm from the surface, where it sharply transitions into a finer-grained precipitate with higher intergranular porosity. From about ~700 μm inwards, the sample microstructure is mostly homogeneous. These microstructures are correlated with a somewhat decreased Ca/Si-ratio in the outer 150–200 μm of the sample. On the sample exposed for 16 weeks, the outer precipitate layer is slightly thicker, and more consistent. Behind it, the degraded zone is ~50 μm wide, before coarse precipitates fill up most porosity. At about 300 μm from the sample surface, the coarse

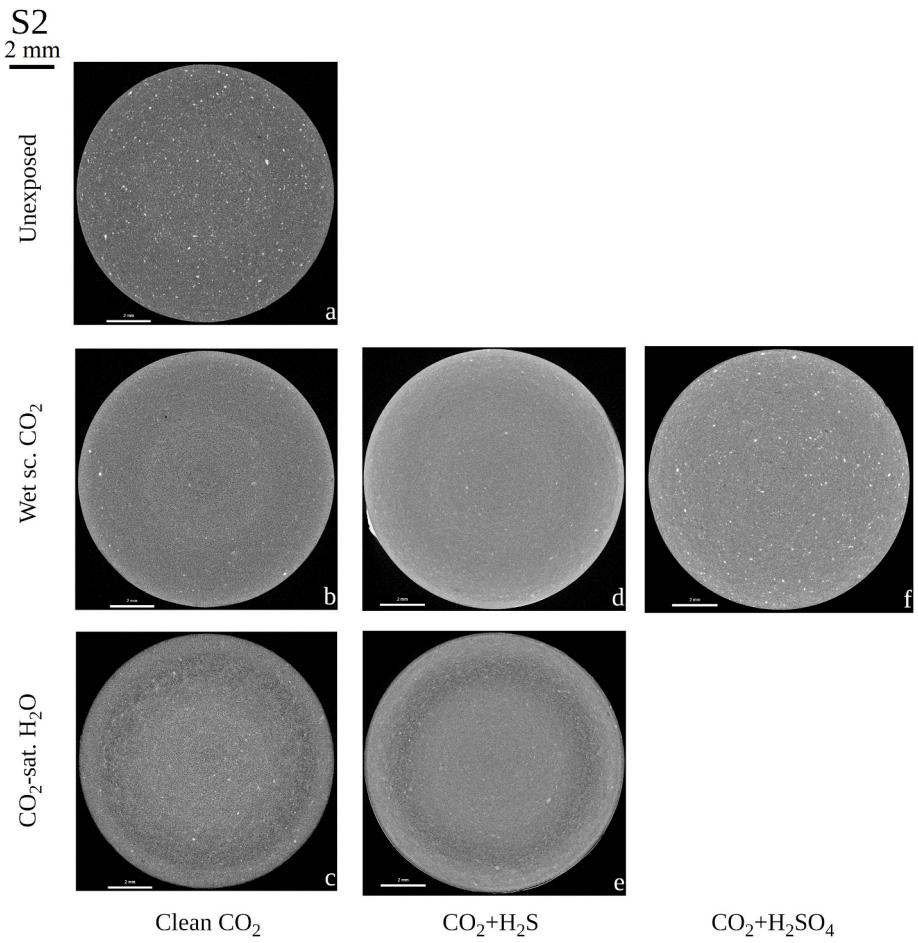

Fig. 8. CT-scans of sealant S2; a) unexposed, b) exposed to wet supercritical CO_2, c) exposed to CO_2-saturated water, d) exposed to wet supercritical CO_2 with 1.6 mol % H_2S, e) exposed to CO_2-saturated water with H_2S, and f) exposed to supercritical CO_2 equilibrated with concentrated H_2SO_4. The scalebars shown with the scans are 2 mm. All exposure durations were 16 weeks. CT scans of the unexposed reference sample and samples exposed to clean CO_2 taken from (van Noort et al., 2025).

precipitates sharply transition to finer precipitates, coarsening inwards between 300 and 650 μm, while from there inwards the microstructure is mostly homogeneous. While the Ca/Si-ratio is somewhat depleted in the outer ~80–100 μm, it is mostly constant (and around the reference value) in the rest of the sample. Both 4 and 16 weeks exposure led to an increase in S/Si-ratio throughout each sample. In these samples submicron high-density particles, similar to those identified as iron sulphides in the S1 samples exposed to CO_2-saturated water, are also observed. In the 4-week exposed sample, these are only found in the outer ~1000 μm, while in the 16-week exposed sample they were found throughout, though mostly in the outer ~600 μm.

Fig. 11 shows cross-sections through S2 samples exposed to supercritical CO_2 in the presence of H_2SO_4 for 4, 8 and 16 weeks. All three samples show an outer zone where carbonation has led to a relatively coarse microstructure, with large pores and massive precipitates. Inwards, this microstructure transitions quite sharply to a zone with very fine, grainy matrix structure, that then gradually coarsens and becomes homogeneous. In the samples exposed for 4 and 8 weeks, the coarse outer zone is ~100–130 μm wide, while the finer microstructure coarsens and becomes homogeneous between ~600 and 800 μm from the sample surface. While in the sample exposed for 4 weeks, the Ca/Si-ratio is mostly constant, in the sample exposed for 8 weeks, this ratio is somewhat depleted up to 500 μm from the sample surface. In the sample exposed for 16 weeks, the coarse outer zone is between 100 and 150 μm wide. Here, the zone with very fine microstructure transitions to a coarser, homogeneous microstructure between ~500 and 800 μm from the sample surface. While the Ca/Si-ratio is depleted in the outer ~50 μm, it is slightly elevated further inwards to 1280 μm from the surface, where it drops sharply to reference values. In all three samples, the S/Si-ratio is somewhat increased over reference values, but does not vary much between surface and centre.

3.4.3. *Sealant S3*

All CT scans of samples of sealant S3 are shown in Fig. 12. The sample exposed to water saturated with clean CO_2 (Fig. 12c) shows relatively little change in density, except for localised areas of density loss within the outer ~200 μm of the sample. In contrast, the sample exposed to water saturated with CO_2 containing H_2S (Fig. 12e) shows a sharply bound outer zone of ~265 μm where its density is increased. Inwards of that zone, the density is somewhat reduced for about ~280 μm, gradually increasing to a constant value (assumed to be unaffected). In the sample exposed to clean, wet supercritical CO_2 (Fig. 12b), the outer rim (~250 μm wide) is somewhat elevated in density, while there are also localised areas of reduced density. Within that, the sample density is somewhat enhanced to ~1100 μm from the sample surface. In the sample exposed to wet supercritical CO_2 with H_2S (Fig. 12d), the outer zone (~310–320 μm wide) is likewise somewhat elevated in density. In the sample exposed to CO_2 with H_2SO_4 (Fig. 12f), a minor increase in density is observed in a relatively wide outer zone, but especially in the outer ~400 μm of the sample.

Fig. 13 shows SEM cross-sections and element ratio curves of sealant S3 samples exposed to CO_2-saturated water, with the CO_2-phase containing 1.6 mol% H_2S, for 4 and 16 weeks. The sample exposed for 4 weeks, shown in Fig. 13a, has a thin outer precipitate layer behind

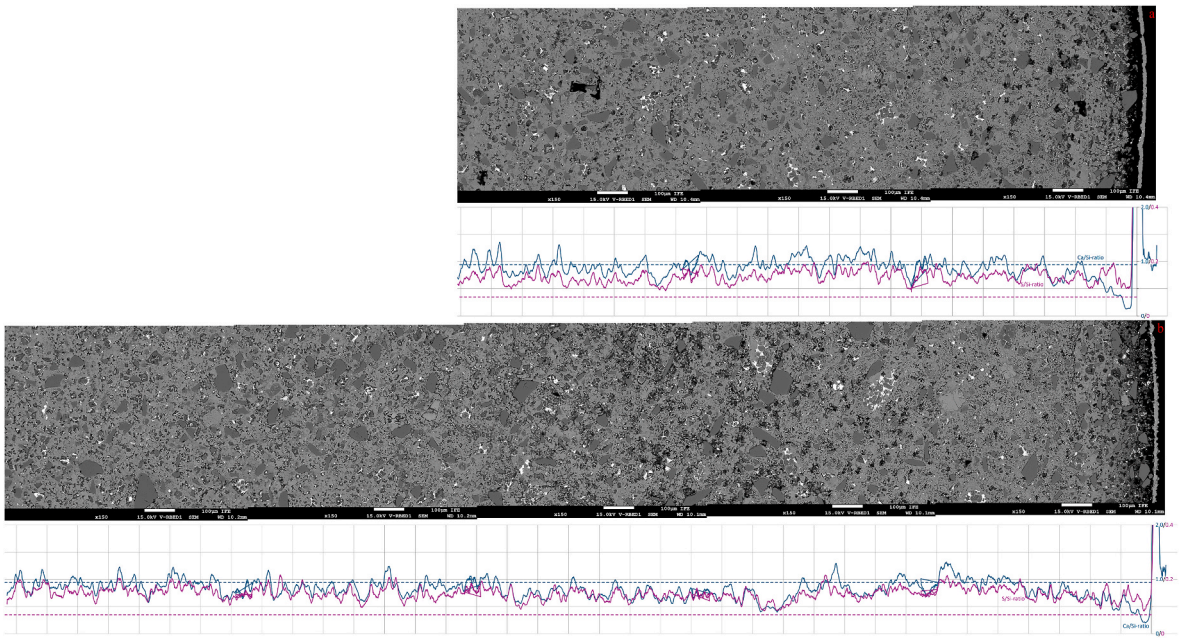

Fig. 9. SEM Micrographs of S2 samples exposed to water saturated with CO_2 containing 1.6 mol% H_2S for 4 (a) and 16 (b) weeks. The graphs underneath each micrograph show the Ca/Si (blue, on the 0–2.0 axis) and S/Si (purple, on the 0–0.4 axis) elemental ratios (atom %/atom %) measured along the micrograph using EDS. The dashed lines are reference values (average values) measured at the centre of an unexposed sample. Scalebars shown with the micrographs and gridline spacing for the graphs are 100 μm.

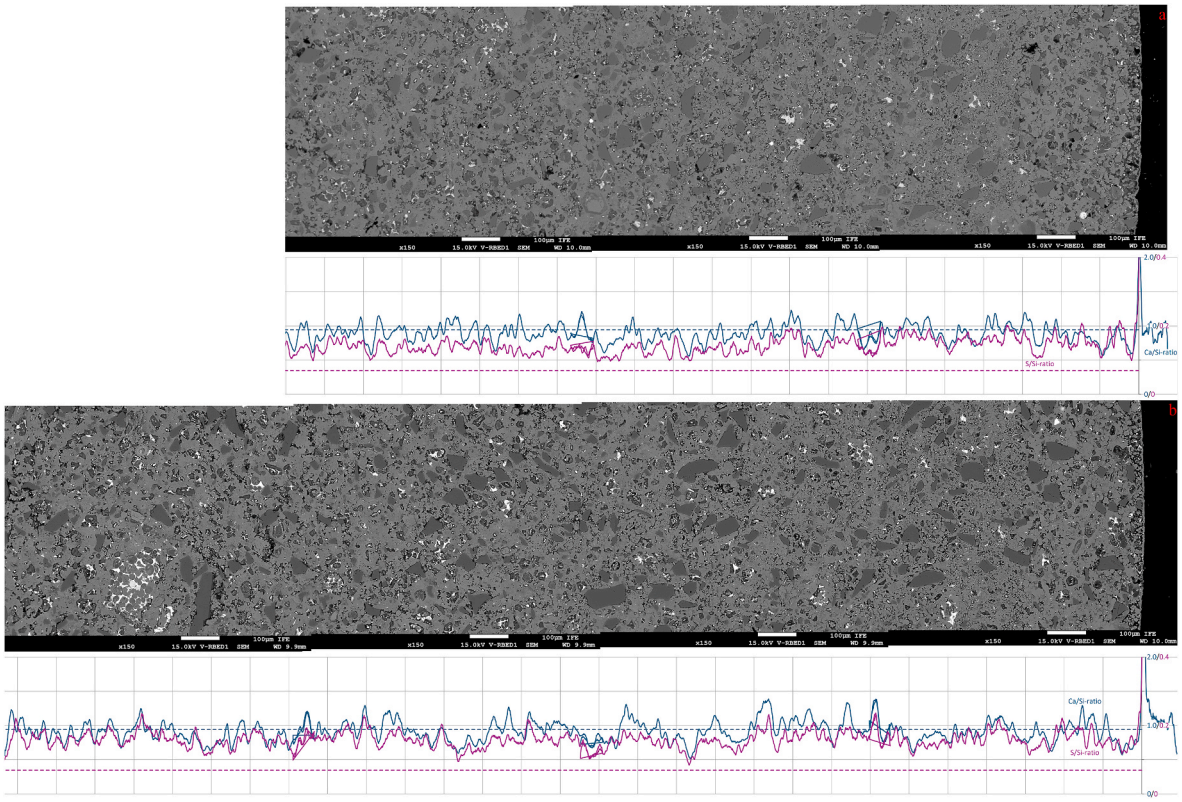

Fig. 10. SEM Micrographs of S2 samples exposed to wet supercritical CO_2 with 1.6 mol% H_2S for 4 (a) and 16 (b) weeks. The graphs underneath each micrograph show the Ca/Si (blue, on the 0–2.0 axis) and S/Si (purple, on the 0–0.4 axis) elemental ratios (atom %/atom %) measured along the micrograph using EDS. The dashed lines are reference values (average values) measured at the centre of an unexposed sample. Scalebars shown with the micrographs and gridline spacing for the graphs are 100 μm.

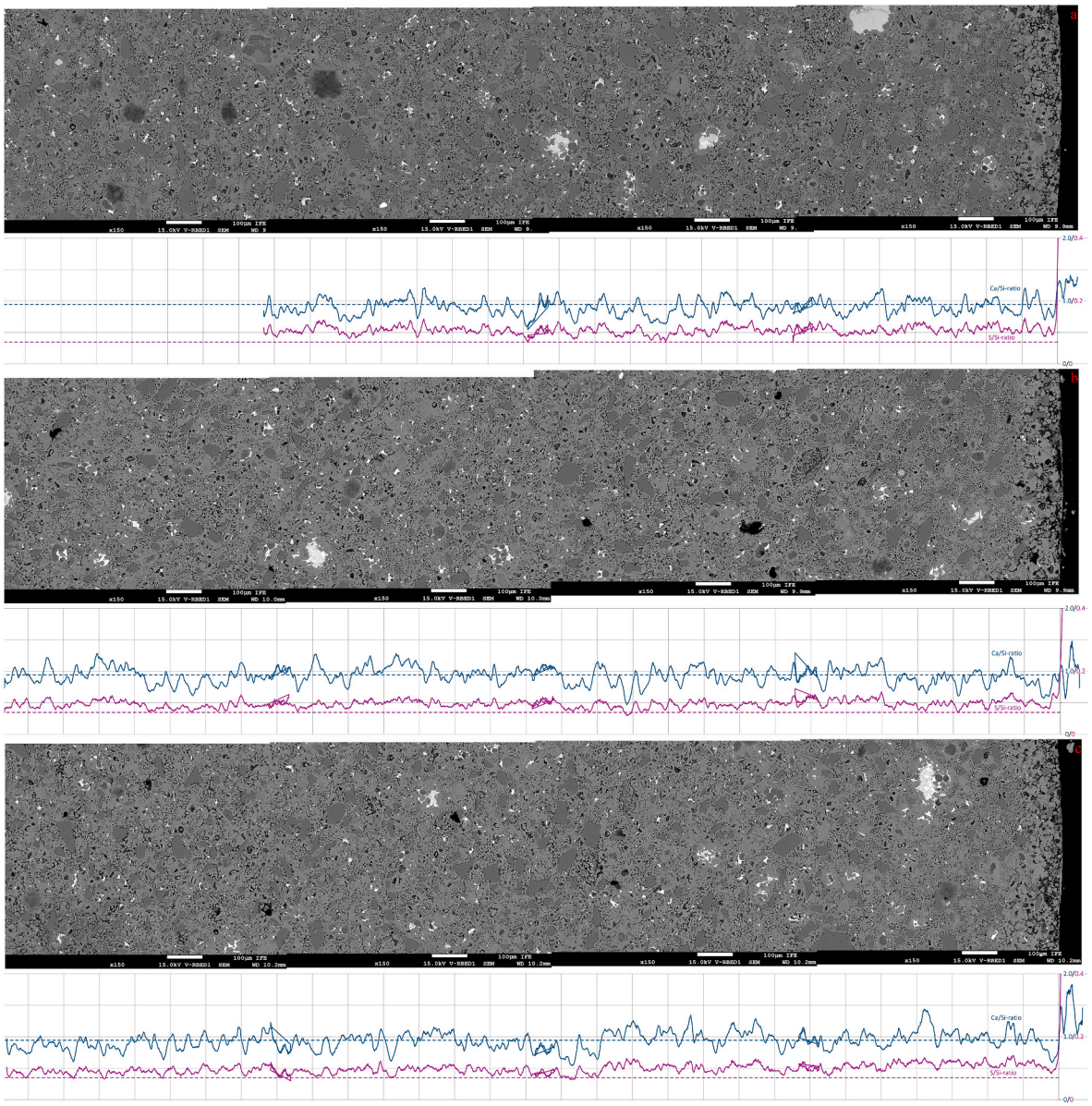

Fig. 11. SEM Micrographs of S2 samples exposed to wet supercritical CO_2 equilibrated with concentrated H_2SO_4 for 4 (a), 8 (b), and 16 (c) weeks. The graphs underneath each micrograph show the Ca/Si (blue, on the 0–2.0 axis) and S/Si (purple, on the 0–0.4 axis) elemental ratios (atom %/atom %) measured along the micrograph using EDS. The dashed lines are reference values (average values) measured at the centre of an unexposed sample. Scalebars shown with the micrographs and gridline spacing for the graphs are 100 μm.

which, over ~50 μm, the sealant is degraded due to dissolution and leaching. Inwards from this, the open pore space is filled with relatively small (<10 μm), spherical precipitates. From ~120 μm, moving inwards this precipitated microstructure coarsens gradually, leading to a relatively coarse, homogeneous microstructure from ~450 μm from the sample surface. In the outer ~100–120 μm, these microstructures are correlated with a somewhat depleted Ca/Si-ratio, and elevated Mg/Ca-ratio. The sample exposed for 16 weeks shows some precipitation on the outer surface. Behind this, the outer ~50–100 μm of the sample is quite degraded. Between ~50 and 400 μm, the pores between larger silicate grains are filled with fine spherical, insular precipitates (<~10 μm in diameter). From ~400 μm inwards, these precipitate grains have relatively dark (i.e., lower in density) cores, and gradually increase in size. From about 1200 μm from the sample surface, the sample microstructure becomes relatively homogeneous, with precipitate rims around larger silicate grains and relatively coarse precipitates in the pore space between these grains. In the outer ~150 μm, the Ca/Si-ratio is depleted (and the Mg/Ca-ratio relatively enriched). From 150 to ~600 μm from the sample surface, the Ca/Si-ratio increases gradually up to reference values. S/Si-ratios are elevated throughout both samples compared to the reference value (0.078), independent of exposure duration (or distance from the sample surface). In these samples sub-micron high-density particles, similar to those identified as iron sulphides in the S1 samples exposed to CO_2-saturated water, are also observed. In the 4-week exposed sample, these are found throughout the exposed sample, but are somewhat more prevalent near the sample surface, while in the 16-week exposed sample they were found throughout, but are considerably more prevalent in a few mm wide zone from ~300 μm from the sample surface.

Fig. 14 shows cross-sections through the S3 samples exposed directly to the H_2S-bearing supercritical CO_2-phase. In the sample exposed for 4 weeks, exposure led to an outer zone with very fine, insular precipitates surrounding the larger silicate grains, with these precipitates coarsening from about ~300–400 μm from the sample surface. Over the outer

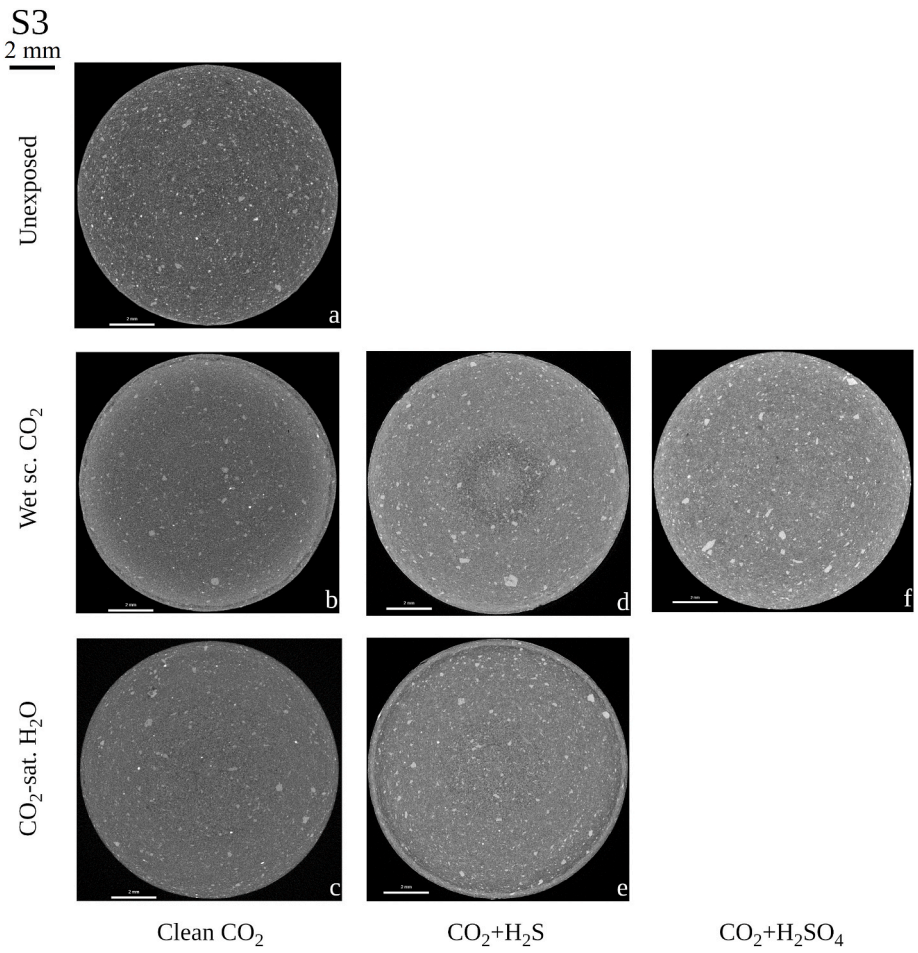

Fig. 12. CT-scans of sealant S3; a) unexposed, b) exposed to wet supercritical CO_2, c) exposed to CO_2-saturated water, d) exposed to wet supercritical CO_2 with 1.6 mol% H_2S, e) exposed to CO_2-saturated water with H_2S, and f) exposed to supercritical CO_2 equilibrated with concentrated H_2SO_4. The scalebars shown with the scans are 2 mm. All exposure durations were 16 weeks. CT scans of the unexposed reference sample and samples exposed to clean CO_2 taken from (van Noort et al., 2025).

~400 μm, the Ca/Si-ratio shows a minor depletion towards the sample surface, while the Mg/Ca-ratio is somewhat elevated. In the sample exposed for 16 weeks, the finer precipitates in the outer zone are considerably less fine than in the sample exposed for 4 weeks (though still <10 μm). Between 200 and 700 μm from the sample surface, these finer precipitates gradually coarsen and become less spherical in shape, leading to a homogeneous microstructure into the sample core. In this sample, the Ca/Si-ratio is significantly depleted in the outer ~100 μm, and somewhat depleted between ~100 and 700 μm, while the Mg/Ca-ratio is somewhat enriched. Furthermore, S/Si-ratios are enriched throughout the samples after both 4- and 16-week exposures. In these samples sub-micron high-density particles, similar to those identified as iron sulphides in the S1 samples exposed to CO_2-saturated water, are also observed. In the 4-week exposed sample, these are found throughout but are somewhat more prevalent in the outer ~2 mm, while in the 16-week exposed sample they were found throughout, but are considerably more prevalent in a few mm wide zone from ~400 μm from the surface.

Fig. 15 shows cross-sections through the S3 samples exposed to supercritical CO_2 containing H_2SO_4, for 4, 8 and 16 weeks. In these samples, exposure resulted in a microstructure in which the larger pre-existing silicate grains (mostly quartz and olivine) are surrounded by a porosity filled with mostly insular precipitate grains (as well as some more continuous precipitates around or between larger grains). The grain-size of the insular precipitates varies in various zones between sample surface and core. In the sample exposed for 4 weeks, in an outer zone of about ~250 μm wide, the precipitate particles are medium in size (~10 μm in diameter), and the open porosity appears somewhat higher than elsewhere in the sample. In this zone, the Ca/Si-ratio is depleted, and then increases sharply to reference values around ~140–150 μm from the sample surface. Inwards of this outer zone, the precipitation found in the pore space is a combination of very fine insular precipitates (typically ~5 μm across) with more massive precipitates around and between the larger silicate grains. However, between ~1600 and ~2100 μm from the sample surface, the finer precipitate is more prevalent, resulting in an apparent lower porosity than in the other parts of the sample. In the sample exposed for 8 weeks, a similar outer zone with relatively high porosity and medium-sized precipitates, ~300 μm wide, is correlated with a somewhat depleted Ca/Si-ratio between ~50 μm and ~200 μm from the sample surface. Inwards of this zone, the precipitates are again a combination of finer, insular grains as well as larger, more massive precipitates mostly around the larger silicate grains. A zone with somewhat decreased porosity due to increased precipitation of fine carbonates, similar to the sample exposed for 4 weeks but less intense, is seen between ~1800 and ~2400 μm from the sample surface. Finally, in the sample exposed for 16 weeks, a similar outer zone of about ~300 μm wide coincides with a somewhat depleted Ca/Si-ratio over the outer ~300 μm. A zone with increased very fine precipitation is observed between ~2200 and 2700 μm from the sample surface. Between these two distinct zones, the sample microstructure is mostly homogeneous. Note that S/Si-ratios are elevated throughout all samples exposed to CO_2 with H_2SO_4.

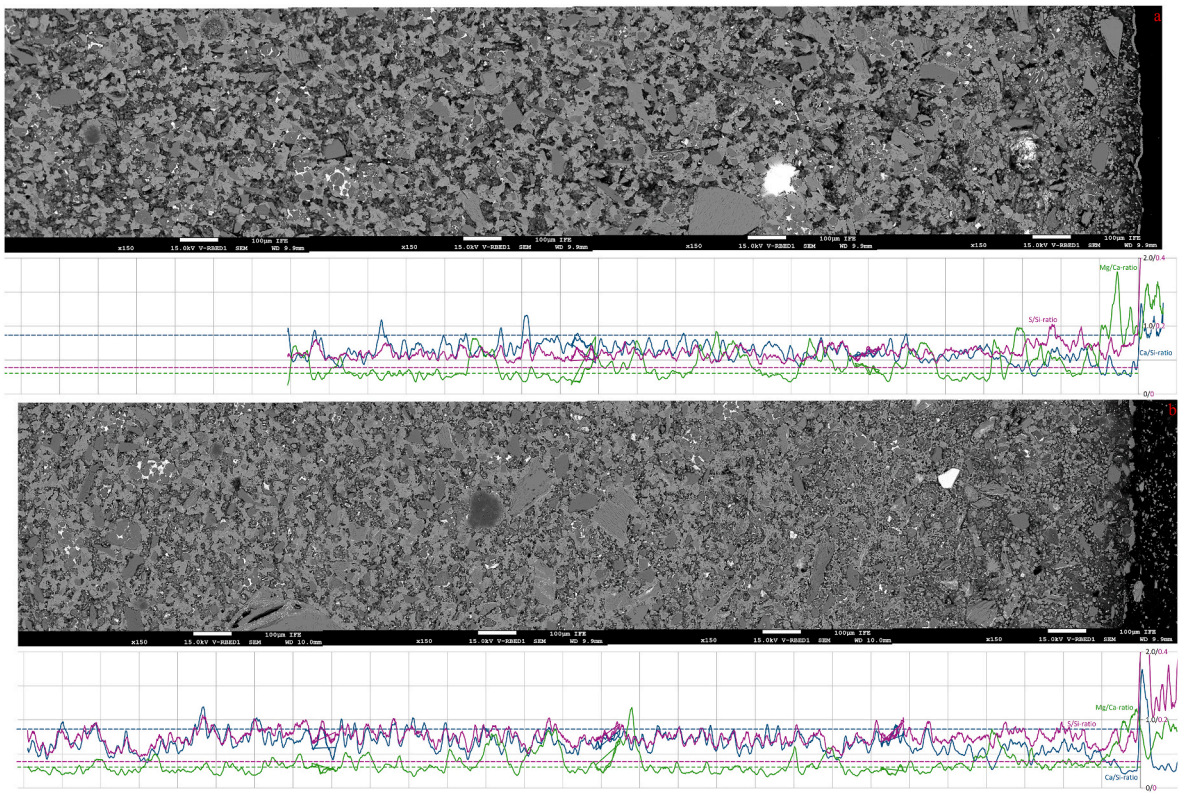

Fig. 13. SEM Micrographs of S3 samples exposed to water saturated with CO_2 containing 1.6 mol% H_2S for 4 (a) and 16 (b) weeks. The graphs underneath each micrograph show the Ca/Si and Mg/Ca (blue and green, respectively, both on the 0–2.0 axis), and S/Si (purple, on the 0–0.4 axis) elemental ratios (atom %/atom %) measured along the micrograph using EDS. The dashed lines are reference values (average values) measured at the centre of an unexposed sample. Scalebars shown with the micrographs and gridline spacing for the graphs are 100 μm.

3.4.4. Sealant S4

All CT scans of samples of sealant S4 are shown in Fig. 16. Here, it is clearly seen that none of the exposures led to significant changes in density, and the samples were not significantly affected by the presence of either H_2S or H_2SO_4.

Similarly to the CT-scans, the SEM cross-sections of S4 samples exposed to CO_2 with H_2S (Figs. 17 and 18) and CO_2 with H_2SO4 (Fig. 19) show that this exposure resulted in only little change in microstructure or composition. No significant microstructural changes are seen in the samples exposed for 4 or 16 weeks to water saturated with CO_2 with H_2S. In the sample exposed for 4 weeks, the Ca/Al- and Si/Al-ratios are somewhat depleted at the sample surface, and rise gradually moving inwards over ~200 μm. In the sample exposed for 16 weeks, such minor depletion is not observed. Though the Si/Al-ratio is somewhat elevated compared to reference values between ~100 μm and ~700 μm from the sample surface, this is also seen in the unexposed samples (van Noort et al., 2025). S/Al-ratios are somewhat elevated compared to the reference value (0.10), notably in the outer ~700 μm of the sample exposed for 16 weeks, but the change is relatively limited.

Direct exposure to wet supercritical CO_2 with H_2S likewise led to limited change in sample microstructure or integrity. However, in the S4 sample exposed thus for 4 weeks, an apparent increase in porosity is observed up to ~600–700 μm from the surface. While this may actually be due to sample preparation differences, this increase in porosity is associated with an elevated Si/Al-ratio peaking at ~200 μm from the sample surface and decreasing gradually to reference values between 200 and 700 μm from the sample surface, as well as an enriched Ca/Al-ratio in the outer ~700 μm of the sample. Note that in the outer 40–50 μm of this sample, the Ca/Al-ratio increases strongly towards the surface, while the Si/Al-ratio decreases. The S/Al-ratio is somewhat enhanced in the outer ~700 μm of this sample. The sample exposed for 16 weeks does not show the somewhat enhanced porosity near the sample surface seen in the sample exposed for 4 weeks. Here, the Si/Al- and Ca/Al-ratios increase strongly in the outer 80–100 μm, to a peak in these ratios, and then decrease gradually going inwards over about 600–700 μm. The S/Al-ratio is somewhat elevated compared to the reference value (0.10), mostly in the outer ~1000 μm.

While some very fine (submicron), high-density particles were observed in S4 samples exposed to CO_2 with H_2S, similar particles were also found in unexposed S4 samples, and samples exposed to clean CO_2, and there was no significant change in quantity of distribution of such particles. The chemical composition of these particles has not been investigated further.

In the samples exposed to supercritical CO_2 with H_2SO_4, likewise no significant changes in sample integrity of microstructure due to exposure are observed. Here, similar, relatively minor variations in Si/Al- and Ca/Al-ratios are observed in the outer ~1000 μm of the samples. S/Al-ratios are somewhat elevated in the outer ~600 μm of the sample exposed for 8 weeks, and the outer ~900–1000 μm of the sample exposed for 16 weeks, while in the sample exposed for 4 weeks, the S/Al-ratios are not affected significantly.

3.4.5. Sealant S5

All CT scans of samples of sealant S5 are shown in Fig. 20. The large irregular holes seen in the unexposed reference sample (Fig. 20a), and in samples of S5 exposed directly to a CO_2-phase most likely formed by the dissolution of activator particles during curing. As noted previously (van Noort et al., 2025), exposure to water saturated with clean CO_2 (Fig. 20c) led to a ~1300–1400 μm wide outer zone with somewhat reduced density, plus a ~1200 μm wide transition to an inner zone with relatively high density. However, density differences between these zones are very minor. Exposure to CO_2-saturated water with H_2S (Fig. 20e) led to a similar outer zone with somewhat reduced density of about 900–1000 μm wide, followed by a ~1900–2000 μm wide irregular

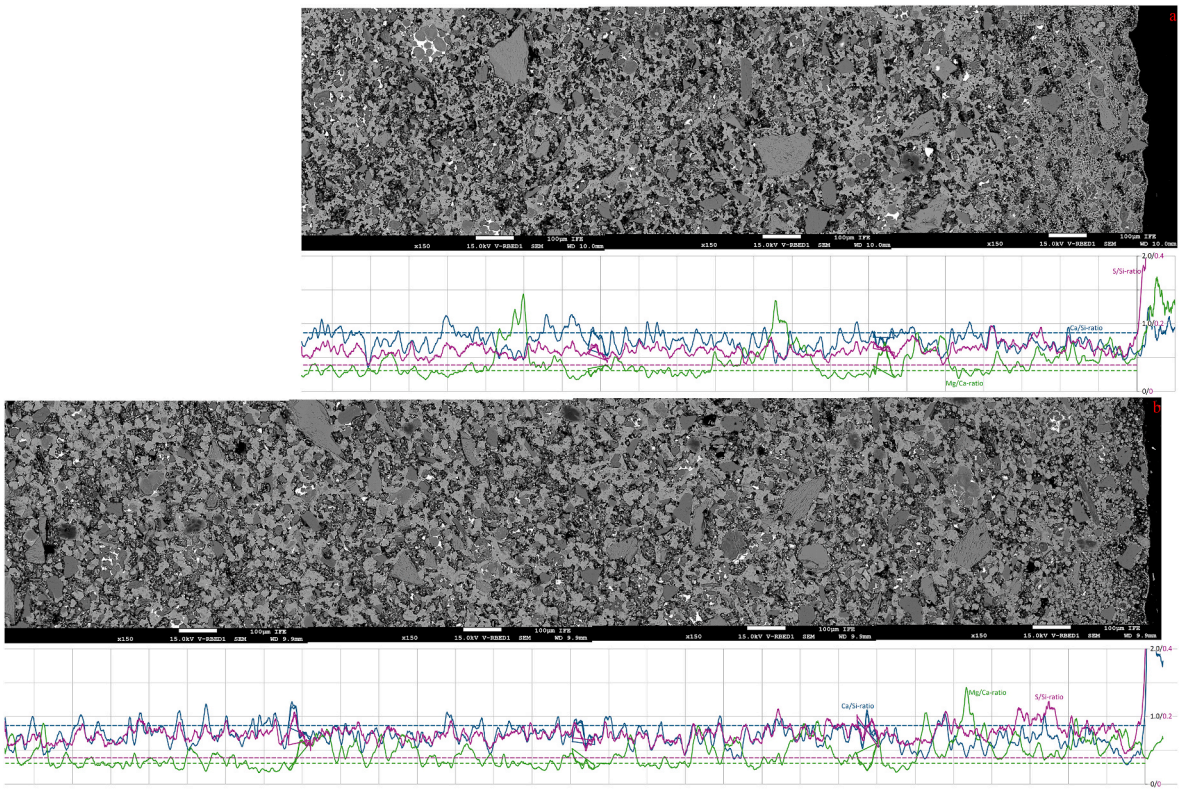

Fig. 14. SEM Micrographs of S3 samples exposed to wet supercritical CO_2 with 1.6 mol% H_2S for 4 (a) and 16 (b) weeks. The graphs underneath each micrograph show the Ca/Si and Mg/Ca (blue and green, respectively, both on the 0–2.0 axis), and S/Si (purple, on the 0–0.4 axis) elemental ratios (atom %/atom %) measured along the micrograph using EDS. The dashed lines are reference values (average values) measured at the centre of an unexposed sample. Scalebars shown with the micrographs and gridline spacing for the graphs are 100 μm.

transition zone. Exposure to wet supercritical CO_2 (Fig. 20b) led to a sharply delineated zone with somewhat enhanced density between ~170 μm and 510 μm from the sample surface, and within that, a diffuse zone with somewhat reduced density. Outside of that zone, near the sample surface, some areas of reduced density are observed. Exposure to wet supercritical CO_2 with H_2S (Fig. 20d) similarly led to enhanced densities in an outer zone ~140–400 μm wide, and within that a slightly reduced density. However, some areas of reduced density are also observed near the sample surface. Exposure to CO_2 with H_2SO_4 (Fig. 20f), however, only resulted in a ~250 μm wide outer rim with slightly enhanced density.

SEM cross-sections of samples exposed to CO_2 with H_2S are presented in Figs. 21 and 22. Considering first the samples exposed to CO_2-saturated water (Fig. 21), in the sample exposed for 4 weeks, in an outer zone of ~100 μm, the matrix is darker, indicating potential degradation. EDS analyses show that in the outer ~650 μm, the Ca/Si-ratio is depleted strongly, then increasing gradually to approximately the reference value at ~1400 μm from the sample surface. The Mg/Si-ratio is likewise somewhat depleted in the outer ~500 μm of the sample. The S/Si-ratio is somewhat elevated near the sample surface compared to the reference value (0.035), decreasing gradually to reference values at ~80 μm from the surface, and then increases somewhat from 600 to 700 μm from the sample surface to remain somewhat elevated further inwards. The sample exposed for 16 weeks has a somewhat dark matrix in the outer ~400 μm. While the Ca/Si-ratio is depleted along the full ~3200 μm analysed, it is most strongly depleted in the outer ~800–900 μm, and increases relatively sharply to near-reference values between 2000 and 2200 μm. The Mg/Si-ratio is likewise depleted somewhat along the full section analysed, though mostly in the outer ~600–700 μm of the sample. The S/Si-ratio is somewhat elevated near the sample surface, decreasing gradually to reference values at ~200 μm from the surface, and then increases somewhat from 900 to 1100 μm from the sample surface to then be consistently elevated further inwards.

In the samples exposed to wet supercritical CO_2 with H_2S (see Fig. 22), after 4 weeks exposure, some precipitation is observed on the sample surface, while in the outer ~100 μm the sample matrix is somewhat darker (i.e., degraded). Furthermore, the Ca/Si-ratio is depleted in the outer ~1000–1100 μm of the sample, as well as from ~1700 μm inwards. The S/Si-ratio is elevated throughout the sample. In the sample exposed for 16 weeks, in the outer ~100 μm the matrix likewise appears somewhat degraded, while between ~100 and ~250 μm from the sample surface, matrix density is enhanced due to carbonate precipitation. The Ca/Si-ratio is somewhat depleted in the outer ~80 μm, but increases rapidly between 60 and 140 μm from the sample surface, and then drops relatively steeply again between 140 and 280 μm. While between ~400 μm and ~1400 μm from the sample surface, the Ca/Si-ratio is somewhat depleted, it then becomes relatively stable inwards at approximately the reference value. The S/Si-ratio is somewhat elevated compared to reference values throughout this sample, in particular in the outer ~200 μm.

Small quantities of very fine (submicron), high-density particles were observed in samples of S5 exposed to CO_2 with H_2S. While these particles appear similar to those identified as Fe-sulphides in samples of S1, S2, and S3 exposed to CO_2 with H_2S, similar particles were also observed in S5 samples exposed to clean CO_2 and the S5 reference sample, and significant differences in quantity or distribution of such particles correlated to exposure fluid composition were not observed.

In the samples exposed to CO_2 in the presence of H_2SO_4 (see Fig. 23) after 4, 8 and 16 weeks, the sample matrixes are somewhat darker in the outer ~100 μm, while Ca/Si-ratios are somewhat depleted there, suggesting minor degradation in this zone. Moving inwards from that, matrix porosities appear somewhat reduced due to carbonate precipitation to ~1200 μm from the sample surfaces. While some precipitation is observed within the matrix inwards from this outer zone, this is not

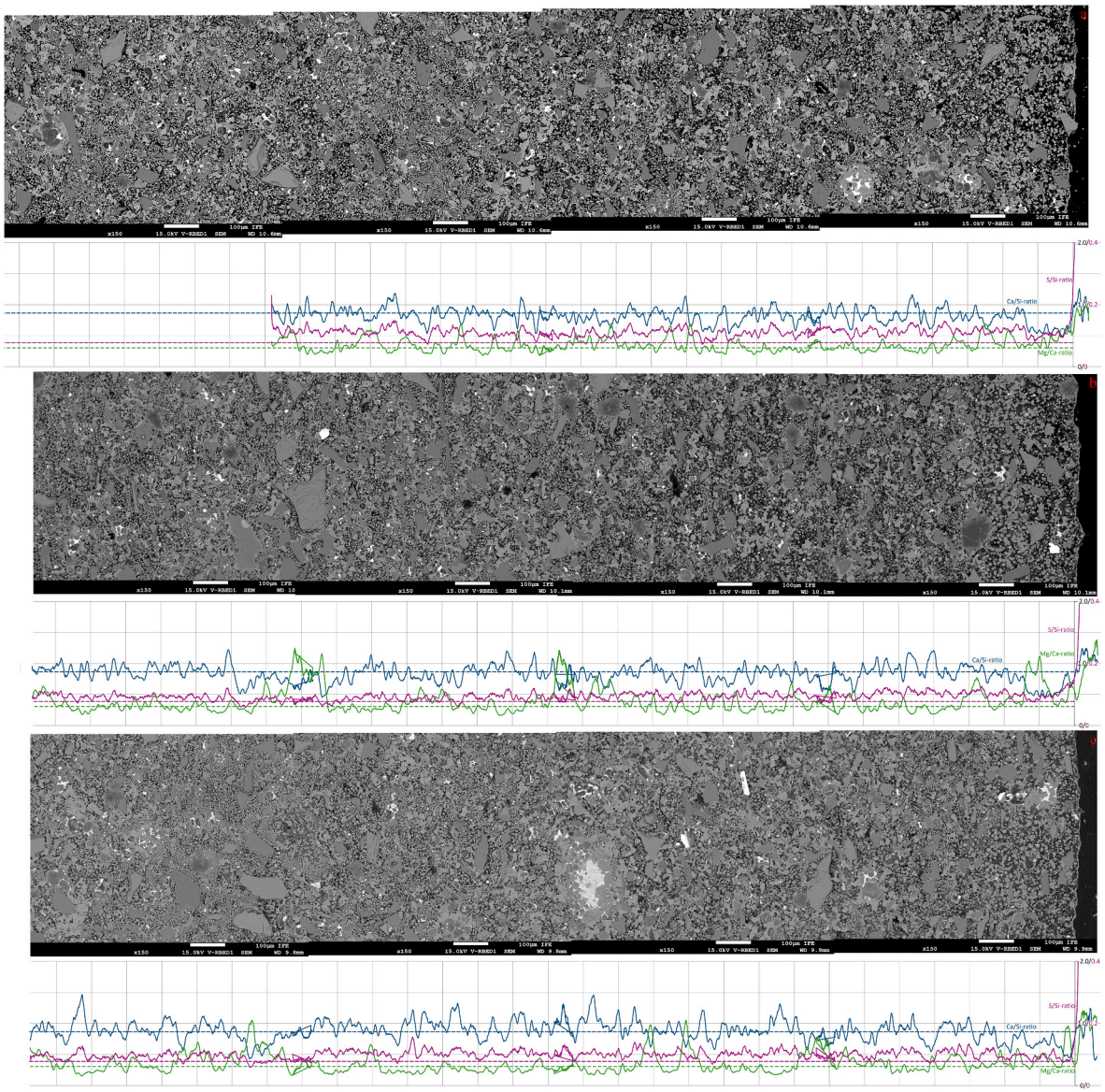

Fig. 15. SEM Micrographs of S3 samples exposed to wet supercritical CO_2 equilibrated with concentrated H_2SO_4 for 4 (a), 8 (b), and 16 (c) weeks. The graphs underneath each micrograph show the Ca/Si and Mg/Ca (blue and green, respectively, both on the 0–2.0 axis), and S/Si (purple, on the 0–0.4 axis) elemental ratios (atom %/atom %) measured along the micrograph using EDS. The dashed lines are reference values (average values) measured at the centre of an unexposed sample. Scalebars shown with the micrographs and gridline spacing for the graphs are 100 μm.

associated with any clear trends in elemental composition. In all three samples, the S/Si-ratio is somewhat elevated, especially in the outer ~200–300 μm.

4. Discussion

4.1. Alteration and degradation of exposed sealants

Based on testing with phenolphthalein on the samples exposed to clean CO_2, free $Ca(OH)_2$ in all tested samples was fully carbonated after only 4 weeks exposure (see also (van Noort et al., 2025)). However, more significant impacts leading to chemical and microstructural alteration and degradation were observed using CT scans (density changes) and SEM/EDS investigation (microstructural changes and significant changes in chemical composition as tracked through elemental ratios). The observed extents of alteration and degradation are displayed in bar diagrams in Figs. 24 and 25.

4.2. Impact of H_2S as impurity in CO_2

While low contents of H_2S in (e.g.,) N_2 are known to impact cement-based sealants quite strongly (cf. (Todorovic et al., 2023)), when exposing sealants to CO_2-saturated water containing H_2S (~0.087 mol %), the overall changes in sealant microstructure and composition are dominated by the impact of CO_2. The most notable impact of H_2S in the experiments reported here was the difference in exposed sample colours, with the presence of H_2S leading to dark blueish colours, whereas exposure to clean CO_2 resulted in more brownish sample colours. Brownish colourations are known to be due to the formation of various (hydr)oxides of (in particular) iron. H_2S is known to react with iron and form black iron sulphides. The difference in exposed sample colours were interpreted as a result of differences in oxidation state during exposure, and the formation of Fe-sulphides and other phases when H_2S was present.

In addition, in sealant S1, the impact of exposure to CO_2-saturated water was enhanced with the addition of H_2S, as seen in the loss of

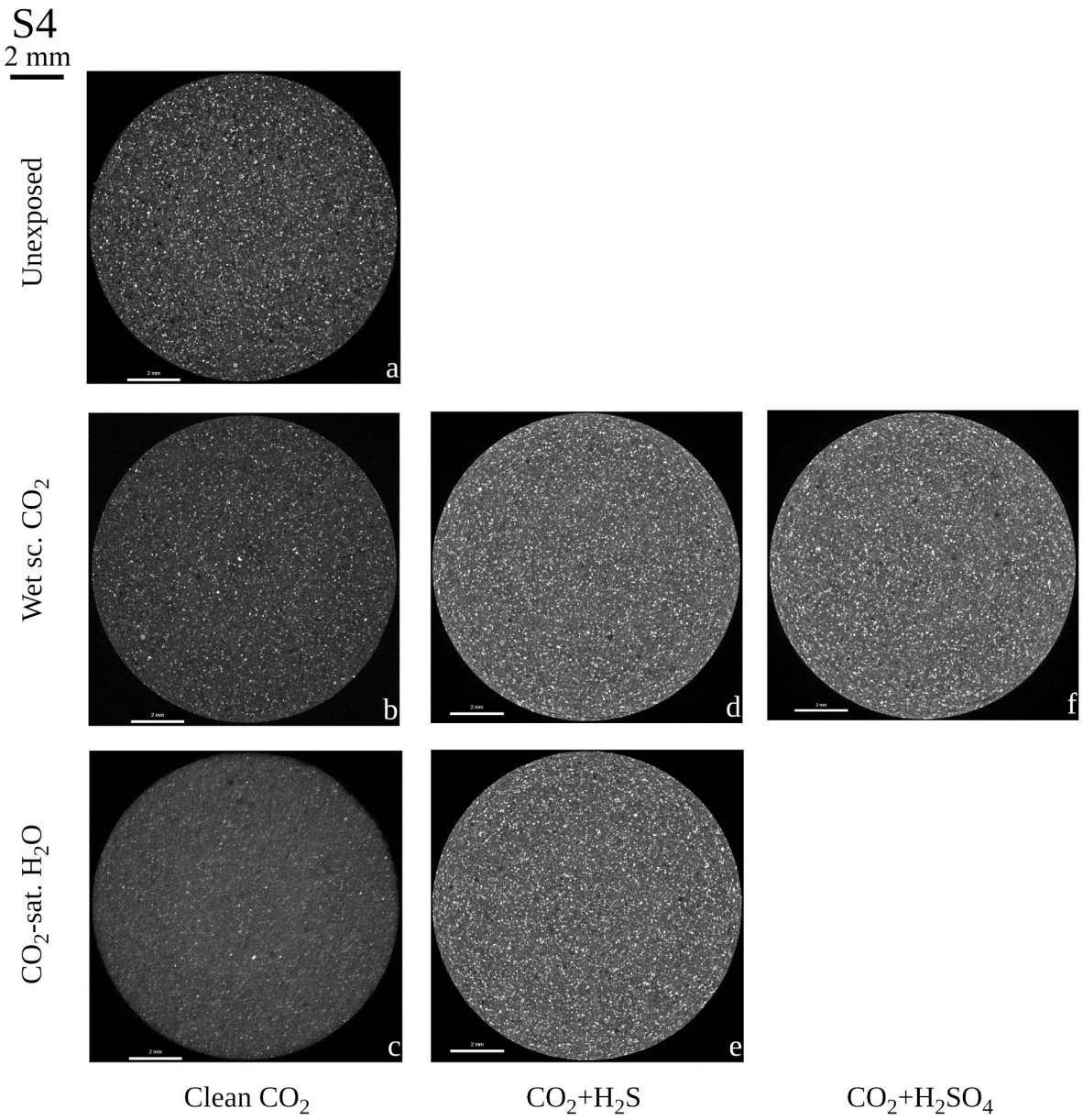

Fig. 16. CT-scans of sealant S4; a) unexposed, b) exposed to wet supercritical CO_2, c) exposed to CO_2-saturated water, d) exposed to wet supercritical CO_2 with 1.6 mol% H_2S, e) exposed to CO_2-saturated water with H_2S, and f) exposed to supercritical CO_2 equilibrated with concentrated H_2SO_4. The scalebars shown with the scans are 2 mm. All exposure durations were 16 weeks. CT scans of the unexposed reference sample and samples exposed to clean CO_2 taken from (van Noort et al., 2025).

sample mass after 16 weeks. This corresponds with increased Ca and Si in solution at the end of the experiment, while with clean CO_2, Ca and Si contents remained constant after 8 weeks, suggesting equilibrium values were maintained. Microstructurally and compositionally, after 16 weeks of exposure, the added impact of H_2S is reflected in a ~1.5 times deeper affected zone where Ca/Si-ratios are depleted more strongly in the presence of H_2S compared to clean CO_2, as seen in both SEM-micrographs and CT-scans.

In sealant S2, the presence of H_2S caused a minor increase in sample mass compared to samples exposed to water saturated with clean CO_2, as well as in fluid Mg-contents (and Na-contents) that are significantly higher. While the microstructural and compositional changes in samples exposed with and without H_2S are similar, based on CT-scanning and SEM analyses, alteration caused by exposure penetrated deeper with H_2S than without H_2S (2100–2200 μm vs. 1800–1900 μm after 16 weeks).

In sealant S3, whereas the sample mass decreased between 8 and 16 weeks exposure times with clean CO_2, it remained relatively constant between 4 and 16 weeks exposure time in the presence of H_2S. Furthermore, fluid Mg-contents after 16 weeks of exposure were much higher in the presence of H_2S, while they remained relatively constant between 4 and 16 weeks without H_2S. Microstructurally, CT-scans show that the presence of H_2S resulted in precipitation and densification in the outer ~265 μm of the sample, as well as some leaching (and reduction of density) just ahead of that enhanced carbonation front. SEM images show that the presence of H_2S resulted in a wider outer zone of degradation and (Ca-)depletion (~100 vs ~50 μm), but also show the higher density of the alteration zone. The total depth of penetration of alteration effects with H_2S was ~1200 μm, while this was estimated to be ~1400 μm for water saturated for clean CO_2. However, it should be noted that as the impact is relatively minor, and the transition is gradual, the exact depth of alteration penetration is hard to assess. Variations in the Ca/Si-ratios mapped using EDS do not show clear differences with or

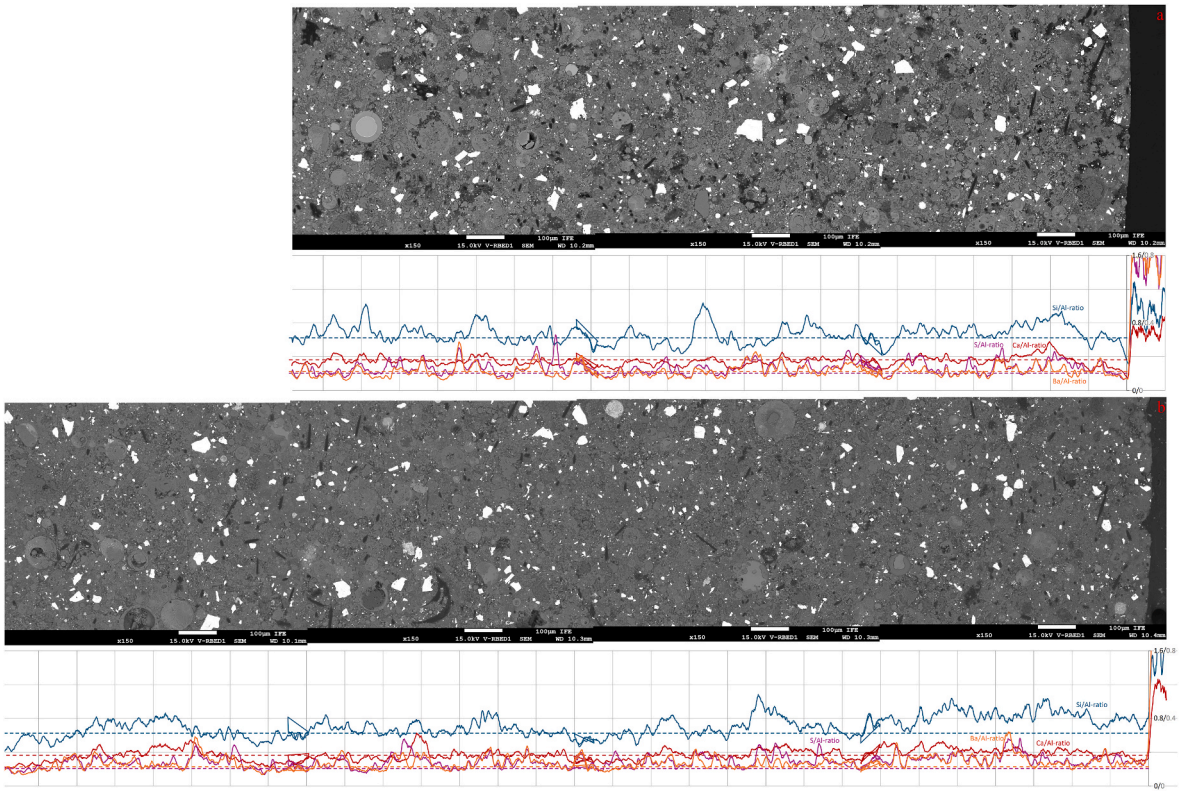

Fig. 17. SEM Micrographs of S4 samples exposed to water saturated with CO_2 containing 1.6 mol% H_2S for 4 (a) and 16 (b) weeks. The graphs underneath each micrograph show the Si/Al and Ca/Al (blue and red, respectively, both on the 0–1.6 axis), and Ba/Al and S/Al (orange and purple, respectively, both on the 0–0.8 axis) elemental ratios (atom %/atom %) measured along the micrograph using EDS. The dashed lines are reference values (average values) measured at the centre of an unexposed sample. Scalebars shown with the micrographs and gridline spacing for the graphs are 100 μm.

without H_2S.

In sealant S4, exposure to CO_2-saturated water in the presence of H_2S did not affect how CO_2-exposure impacted the sealants in terms of chemical, microstructural, or mass changes. In sealant S5, the presence of H_2S lead to an increase in the depth to which the sample was (somewhat) degraded, from ~200 to ~400 μm after 16 weeks. While exposure to water saturated with clean CO_2 and water saturated with CO_2 with H_2S both lead to a depletion of the Ca/Si-ratio deep into the sample, this was not associated with any visible impacts on sealant microstructure or integrity.

Compared to exposure to water saturated with clean CO_2, the most significant impact of H_2S is to somewhat enhance the changes induced by CO_2, and in particular the penetration depth of these effects in sealant samples based on PC. In sealants where the impact of exposure to CO_2-saturated water was limited or negligible (S4 and S5), a 1.6 mol% H_2S-content in the CO_2-phase also has negligible to limited additional impact on sealant microstructure.

While chemical composition measurements of the hydrous exposure fluid were mostly consistent between exposures to clean CO_2 and exposures to CO_2 with H_2S, some interesting differences were observed. Most notable are the significantly elevated concentrations of Mg for S1, S2 and S3, as well as elevated concentrations of Si and Ca for S1. For clean CO_2, fluid concentrations of these elements were constant between 8 and 16 weeks, suggesting an equilibrium between precipitation and dissolution was attained. Thus, the significantly higher concentrations of these elements after 16 weeks exposure with H_2S implies that the presence of H_2S caused a shift in this equilibrium, by inhibiting precipitation of these elements as carbonates (and silica) or enhancing subsequent dissolution of precipitates. For S1, this is indeed confirmed through the lower Ca/Si-ratios in the samples exposed to CO_2 with H_2S, as well as the much less prevalent carbonate precipitation seen in both CT-scans and SEM micrographs. As Mg-carbonates (or other Mg-bearing precipitate phases) were not observed directly, an inhibition of Mg-bearing minerals cannot be confirmed directly. As the reaction between H_2S and (dissolved) Fe^{2+} to form pyrite can generate H^+ (cf. (Talman, 2015)), the resulting acidification is a potential mechanism by which H_2S could lead to reduced carbonate precipitation.

In addition, ICP-OES analyses showed higher S-contents in the exposure fluids of S1, S2 and S3 after exposure to CO_2 with H_2S compared to clean CO_2. However, the S-concentrations in all exposure fluids were considerably lower than the calculated equilibrium concentration, suggesting that sulphur was removed from the fluid through interaction with the sealant samples. While in samples of S1, S2, and S3 exposed to CO_2 with H_2S, Fe-sulphide particles were identified, no newly-formed S-binding minerals were identified in sealants S4 and S5 in this study.

In sealant samples exposed directly to wet supercritical CO_2, for most compositions tested, the presence of H_2S only had a limited impact on how the samples were affected, as assessed through mass changes, microstructural observations, and chemical mapping using EDS. CT-scans show that in sealant S1, the presence of H_2S caused the densification near the outer surface of the samples, ascribed to carbonate precipitation, to be more pronounced, but restricted to a narrower zone. To the contrary, in sealant S2 the presence of H_2S resulted in a more distributed density alteration, with less intense precipitates distributed deeper into the sample. In both these sealants, the presence of H_2S resulted in less enhanced carbonate precipitation (i.e., densification) in the outer parts of the exposed sample than observed after exposure to clean CO_2. While for S1, alteration depths were somewhat enhanced in the presence of H_2S (620 μm compared to 500 μm with clean CO_2, after 16 weeks), for sealant S2, alteration depths when exposed to wet supercritical CO_2 containing H_2S were lower (700 μm compared to 1020 μm with clean CO_2, after 16 weeks). In sealant S4, the presence of H_2S had no impact on the exposed samples. In sealant S5, CT-scans show that

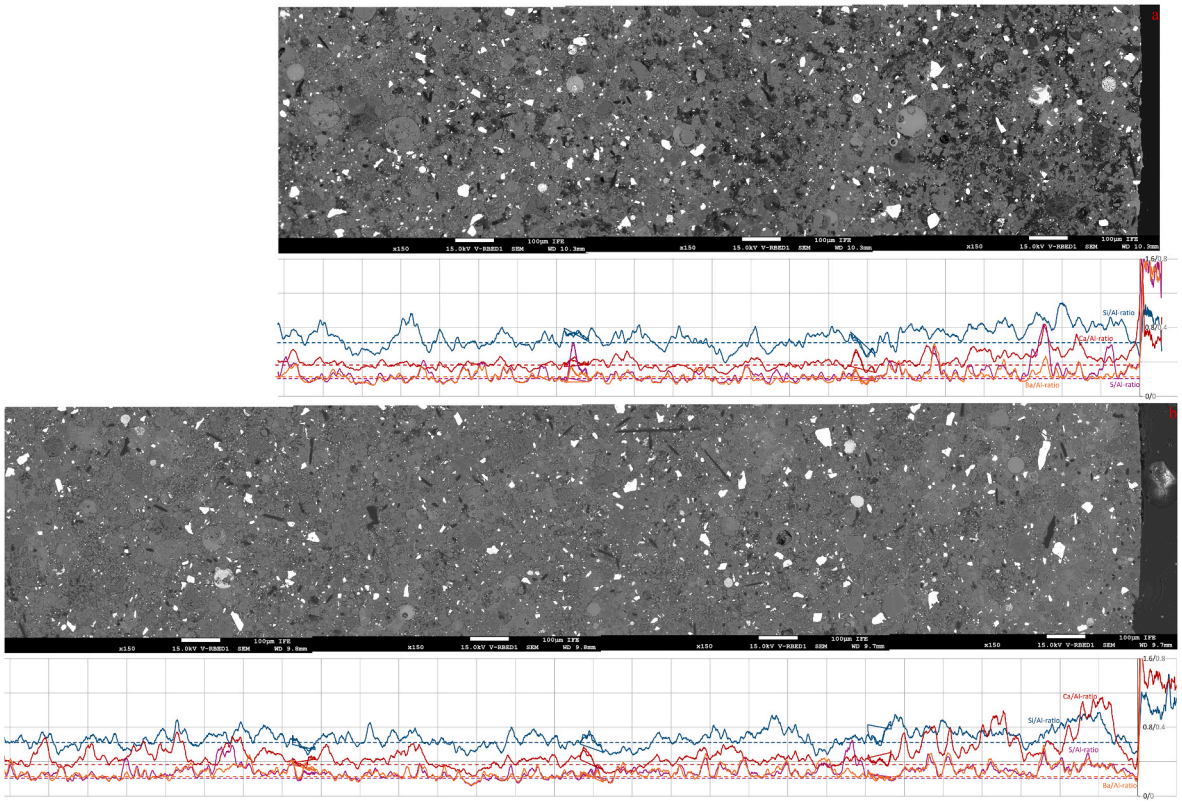

Fig. 18. SEM Micrographs of S4 samples exposed to wet supercritical CO_2 with 1.6 mol% H_2S for 4 (a) and 16 (b) weeks. The graphs underneath each micrograph show the Si/Al and Ca/Al (blue and red, respectively, both on the 0–1.6 axis), and Ba/Al and S/Al (orange and purple, respectively, both on the 0–0.8 axis) elemental ratios (atom %/atom %) measured along the micrograph using EDS. The dashed lines are reference values (average values) measured at the centre of an unexposed sample. Scalebars shown with the micrographs and gridline spacing for the graphs are 100 μm.

carbonate precipitation near the surface of the sample, observed as a local increase in density, is more enhanced in the presence of H_2S. Based on SEM images, after exposure to clean CO_2, precipitation is concentrated between ~70 and 400 μm from the sample surface, while in the presence of H_2S, this is limited to a considerably narrower band between 100 and 250 μm from the surface. Based on chemical compositions, in particular depletion of the Ca/Si-ratio, S5 was altered to a greater depth in the presence of H_2S than with clean CO_2 (1400 vs 960 μm).

In sealant S3, the presence of H_2S during exposure to wet supercritical CO_2 had a more complicated impact. In CT-scanning, the sample exposed to clean CO_2 showed a thin outer zone with enhanced carbonation, inwards of which a zone of reduced density was found giving the appearance of a carbonated outer shell detaching from the sample. Inwards from this, densities were enhanced again, and then dissipated towards the centre. In the sample exposed to CO_2 with H_2S, the outer zone only shows increased density, which then dissipates inwards. While the SEM images of the sample exposed to clean CO_2 clearly show a decreased porosity due to precipitation between ~300 and 1200 μm from the surface, associated with an increasing Ca/Si-ratio, in the sample exposed to CO_2 with H_2S, reduced porosities due to precipitation are only observed between ~50 and 200 μm. Ca/Si-ratios show similar depleted trends in both samples. Overall, the observed alteration depth in the presence of H_2S (after 16 weeks) was lower than for clean CO_2 (700 vs. 1320 μm).

In all PC-based sealants (S1-S3), the S/Si-ratio was elevated throughout the sample, indicating full penetration of S-bearing fluids, for both exposure to CO_2-saturated water and exposure to wet supercritical CO_2. For the S2 and S3 samples, the elevated S/Si-ratios did not depend on exposure duration (4 vs. 16 weeks) or exposure conditions (i.e., whether they were exposed to wet supercritical CO_2 or CO_2-saturated water). However, in the S1 samples exposed to wet supercritical CO_2, while the S/Si-ratios are elevated throughout (and to similar values for the 4- and 16-week exposures), the S/Si-ratios are even higher in the outer 100–150 μm (4-week) to 400 μm (16-week). In the S1-sample exposed to CO_2-saturated water for 16 weeks, S/Si-ratios are likewise elevated throughout. However, they are less elevated in the depleted zone where Ca/Si-ratios are also depleted, and then rise further inwards of this zone (from ~2700 μm from the surface). In the sample exposed for 4 weeks, the S/Si-ratios are similarly less elevated in the depleted outer ~500 μm, and less elevated throughout than in the sample exposed for 16 weeks. Furthermore, in the S1 samples tested, the S/Si-ratios are most elevated in the sample exposed to CO_2-saturated water, but the S/Si-ratios in the depleted zone of these samples are lower than the ratios measured in the samples exposed to wet supercritical CO_2.

In sealant S5, exposure to wet supercritical CO_2 with H_2S led to elevated S/Si-ratios throughout the samples. In the S5 sample exposed for 4 weeks, the S/Si-ratio is independent of distance from the contact surface, while in the sample exposed for 16 weeks, the S/Si-ratio is somewhat further elevated in the outer ~200 μm. After exposure to CO_2-saturated water with H_2S, S/Si-ratios were elevated in the outer ~80 μm (4-week exposure) to 200 μm (16-week exposure), decreasing inwards to the reference value (or just below that). Then, S/Si-ratios were elevated again from 600 to 700 μm (4-week exposure) or 900–1100 μm (16-week exposure) from the surface. Comparing exposure to CO_2-saturated water to wet supercritical CO_2, the S/Si-ratios after 16 weeks were somewhat higher in the outer ~1000 μm of the sample exposed to wet supercritical CO_2, while further inwards the S/Si-ratios were similar. Minor increases in the S/Al-ratio were also observed for S4 sealants exposed to CO_2 with H_2S, mostly in the outer 700–1000 μm of these samples.

These measurements show that sulphur penetrated quite deeply into most sealants. For the PC- based sealants (S1-S3), submicron high-

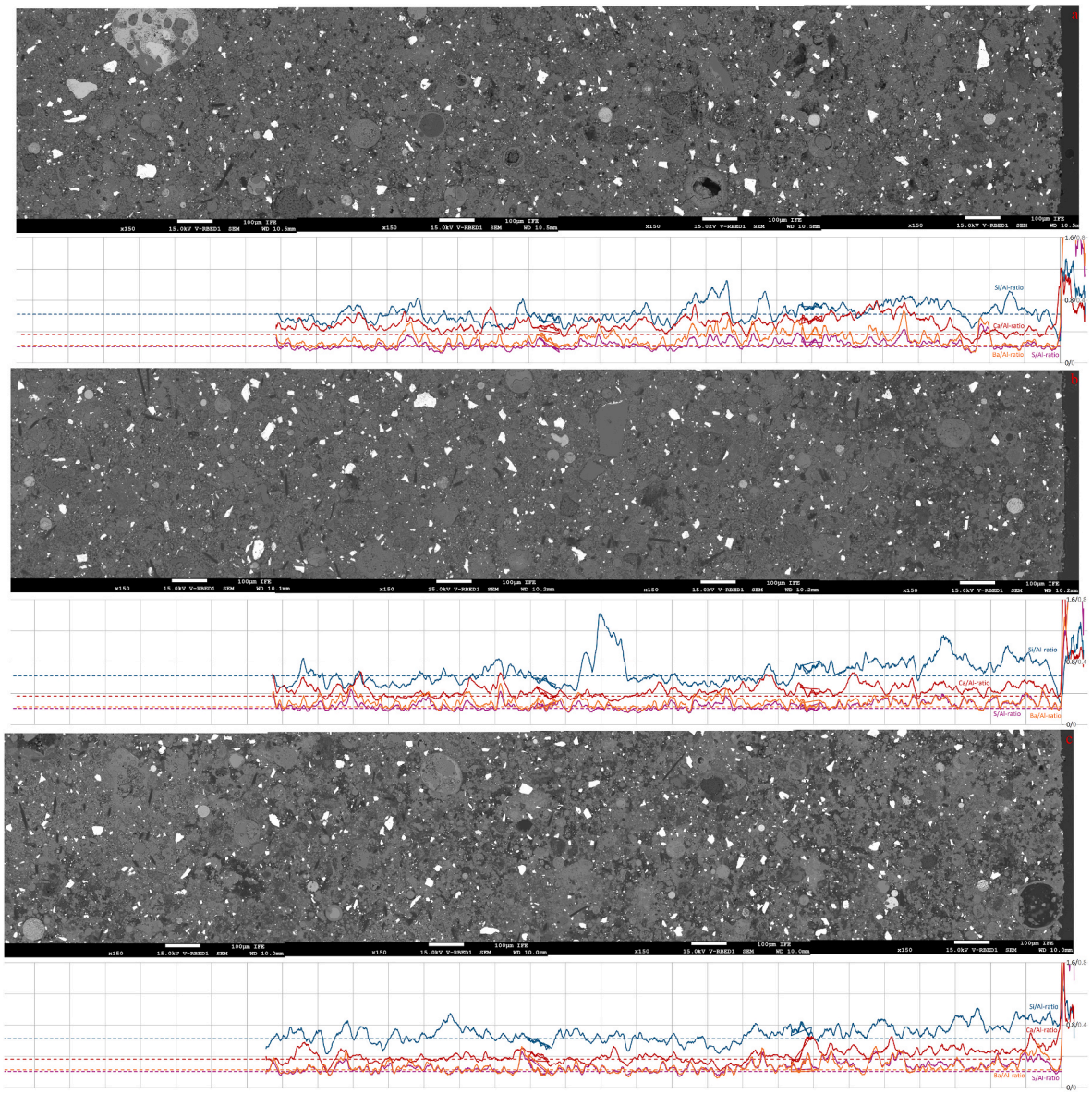

Fig. 19. SEM Micrographs of S4 samples exposed to wet supercritical CO_2 equilibrated with concentrated H_2SO_4 for 4 (a), 8 (b), and 16 (c) weeks. The graphs underneath each micrograph show the Si/Al and Ca/Al (blue and red, respectively, both on the 0–1.6 axis), and Ba/Al and S/Al (orange and purple, respectively, both on the 0–0.8 axis) elemental ratios (atom %/atom %) measured along the micrograph using EDS. The dashed lines are reference values (average values) measured at the centre of an unexposed sample. Scalebars shown with the micrographs and gridline spacing for the graphs are 100 μm.

density particles were observed in the exposed samples using SEM. Based on EDS-analysis of such particles in the S1 sample exposed to CO_2-saturated water with H_2S for 16 weeks, at least part of the sulphur penetrating these samples precipitated as Fe-sulphides. More detailed SEM studies, combined with XRD analysis could be used to assert whether other sulphide minerals also formed.

(van Noort et al., 2025) derived and reported extrapolations of the depths to which their samples were affected after exposure to clean CO_2. While the data obtained here for exposure to CO_2 with 1.6 mol% H_2S is insufficient to attempt a similar extrapolation, comparison to the samples exposed by Van Noort et al. shows that in general the samples exposed to CO_2 with H_2S are affected to similar depths (between about 0.5 and 2 times) as those of equivalent samples exposed to clean CO_2. Based on the available data, estimated extrapolations to 30 years fall within one order of magnitude from the given extrapolations for clean CO_2. However, it must be kept in mind that these extrapolations to 30 years exposure based on single exposure experiments with a total duration of 16 weeks carry very large uncertainties.

4.3. Impact of H_2SO_4 as impurity in CO_2

SO_x has been identified as a key impurity with potential high reactivity with reservoir minerals, reservoir fluids and wellbore cements when co-injected with CO_2. SO_x can react with water and other impurities to form H_2SO_4 (Morland et al., 2019a,b), which is a strong acid. As H_2SO_4 partitions into the hydrous phase, this can cause strong acidification of the hydrous fluids near the injection point, including in the pore fluids trapped in exposed sealants.

To simulate the presence of relatively large quantities of H_2SO_4 at a low concentration in the CO_2-phase, wet sealant samples were exposed to supercritical CO_2 in the presence of vials of concentrated sulphuric acid. Unfortunately, while this enabled simulation of exposure under realistic conditions, the saturated solutions of H_2SO_4 also acted as drying agents, removing water from the initially water-saturated sealant samples. Based on drying tests, the sealants had water-contents of 21–25 wt. %. Comparing sample mass changes for the H_2SO_4-exposed samples to samples exposed to wet supercritical CO_2 (without H_2S), indicates

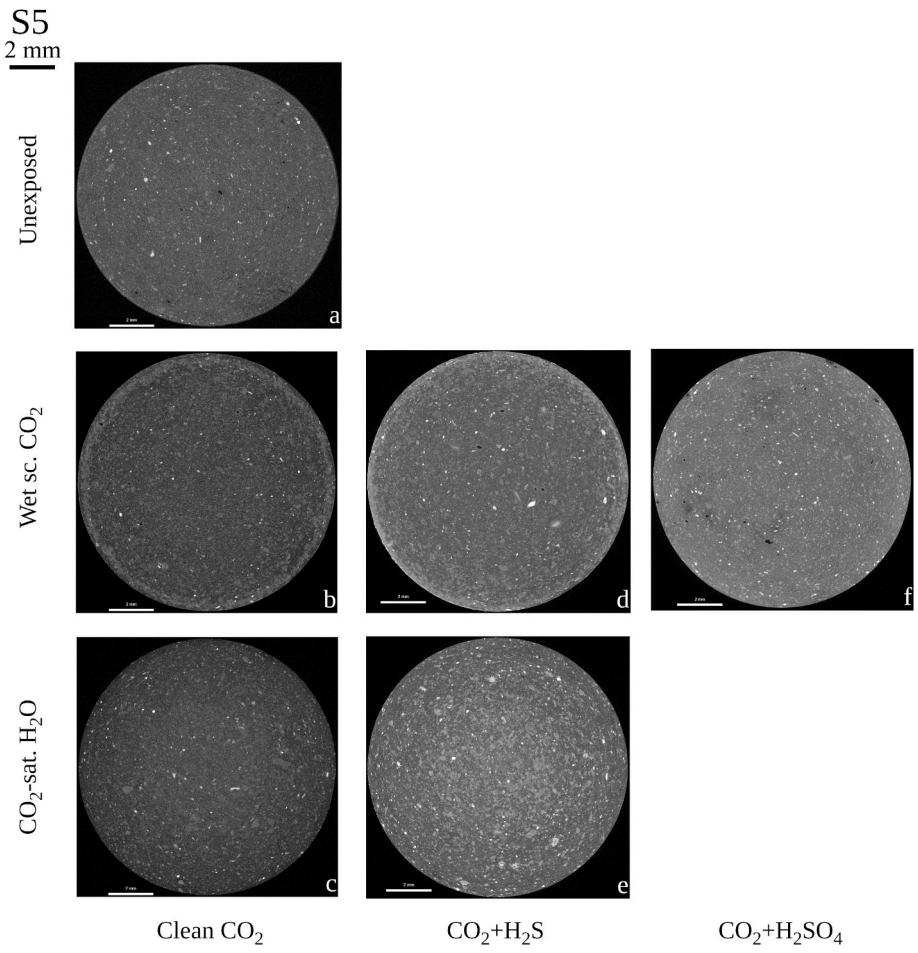

Fig. 20. CT-scans of sealant S5; a) unexposed, b) exposed to wet supercritical CO_2, c) exposed to CO_2-saturated, d) exposed to wet supercritical CO_2 with 1.6 mol% H_2S, e) exposed to CO_2-saturated water with H_2S, and f) exposed to supercritical CO_2 equilibrated with concentrated H_2SO_4. The scalebars shown with the scans are 2 mm. All exposure durations were 16 weeks. CT scans of the unexposed reference sample and samples exposed to clean CO_2 taken from (van Noort et al., 2025).

exposed samples masses after 16 weeks that are 8–18 % lower (see Table 4). Under the assumption that the increase in mass due to carbonation for these samples is similar, this would indicate that during the H_2SO_4-exposure tests, the exposed samples did not dry out completely (though for S4 the remaining water content would be very low).

As sample mass change in these samples is a combination of the precipitation of carbonates (and sulphates) leading to an increase in mass, as well as the evaporation of pore water leading to a decrease in mass, a relatively small reduction in sample mass compared to the measured water content can also indicate a larger decrease due to dehydration compensated by a larger increase due to precipitation. However, considering the CT-scans and SEM images presented above, there are no indications that the presence of H_2SO_4 led to such a significant enhancement in carbonation compared to clean CO_2. Note that for sealants S4 and S5, exposure to clean, wet supercritical CO_2 did not lead to any significant changes in sample mass, meaning that the changes in sample mass observed in the samples exposed with H_2SO_4 mostly represent dehydration. Furthermore, note that sample dehydration also explains the observed "bleaching" of the outer surfaces of these samples after exposure, while drying induced shrinkage could explain the brittle behaviour of S1 and S2 samples during cross-sectioning.

CT-scanning of the S1 sample exposed for 16 weeks shows a more diffuse, less intense densification of the outer part of this sample compared to S1 samples exposed to clean CO_2 or CO_2 with H_2S. Furthermore, the scan shows some inhomogeneity in density in the outer ~100 μm. SEM imaging of the S1 sample exposed to CO_2 with H_2SO_4 (for 16 weeks) shows minor degradation in the outer ~150 μm of this sample. Such degradation was not observed in the S1 samples exposed to clean wet supercritical CO_2 or CO_2 with H_2S for 16 weeks, though it was observed in S1 samples exposed to clean CO_2 or CO_2 with H_2S for 4 or 8 weeks. The degradation (increased porosity) is associated with a depleted Ca/Si-ratio in the outer 80–100 μm of this sample. The same is observed for the S2 sample exposed to CO_2 with H_2SO_4, where CT-scanning shows more diffuse densification, while SEM observations show minor degradation in the outer 100–150 μm, associated with a minor decrease in the Ca/Si-ratio in the outer 50 μm, and reduced porosity due to enhanced carbonation up to ~800 μm into the sample, deeper than observed in the samples exposed to clean CO_2, or CO_2 with H_2S. In sealant S3, exposure to CO_2 with H_2SO_4 likewise resulted in more diffuse, deeper-reaching carbonation than exposure to clean CO_2 or CO_2 with H_2S.

A potential explanation for the lack of carbonate precipitation in the outer part of the S1 and S2 samples exposed to CO_2 with H_2SO_4 is that in these samples, drying out prevented the dissolution-precipitation reactions necessary for carbonation to take place. This drying out would then lead to deeper penetration of CO_2 through the dried pore network before CO_2-dissolution into pore fluids remaining deeper within the samples would lead to carbonate precipitation there, which would explain the deeper and more diffuse carbonation observed in these three samples. An alternative explanation for the reduction in carbonate precipitation observed in these samples is that this was inhibited as a result of acidification caused by the H_2SO_4.

In sealant S5, CT-scanning shows that the sample exposed to CO_2

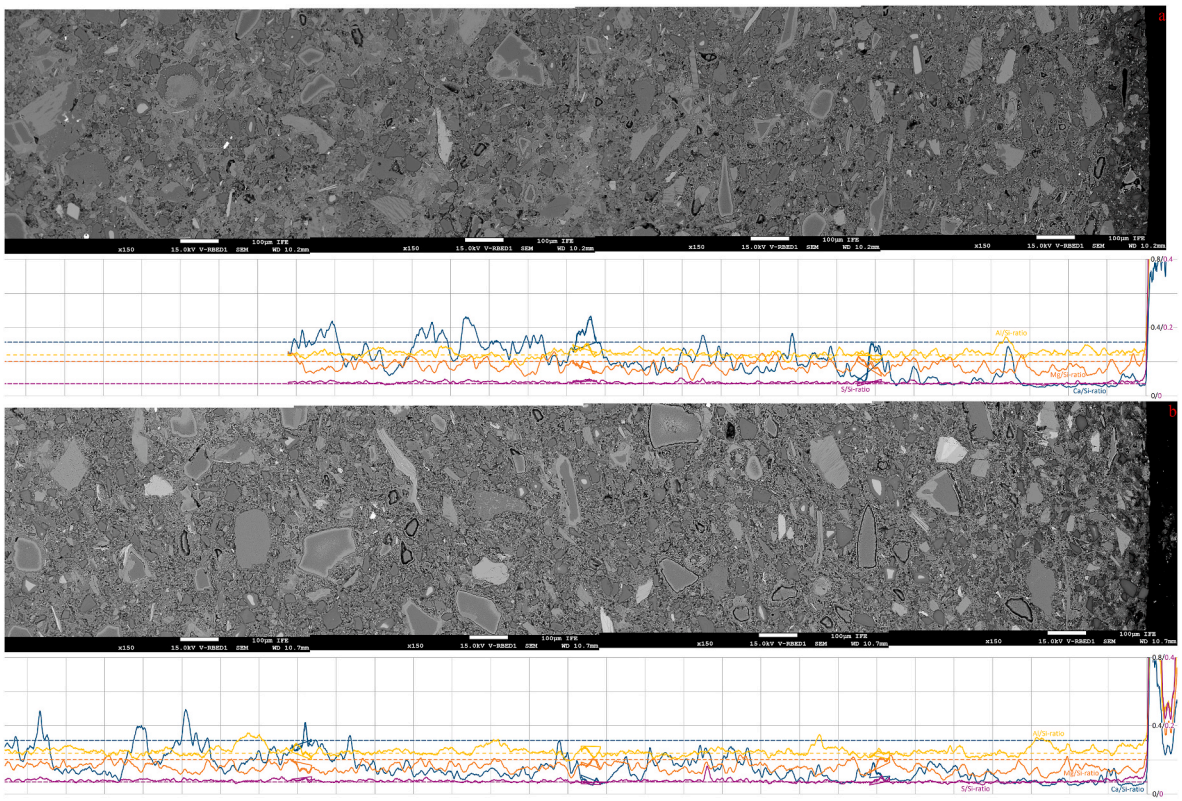

Fig. 21. SEM Micrographs of S5 samples exposed to water saturated with CO_2 containing 1.6 mol% H_2S for 4 (a) and 16 (b) weeks. The graphs underneath each micrograph show the Ca/Si, Mg/Si and Al/Si (blue, orange and yellow, respectively, all on the 0–0.8 axis), and S/Si (purple, on the 0–0.4 axis) elemental ratios (atom %/atom %) measured along the micrograph using EDS. The dashed lines are reference values (average values) measured at the centre of an unexposed sample. Scalebars shown with the micrographs and gridline spacing for the graphs are 100 μm.

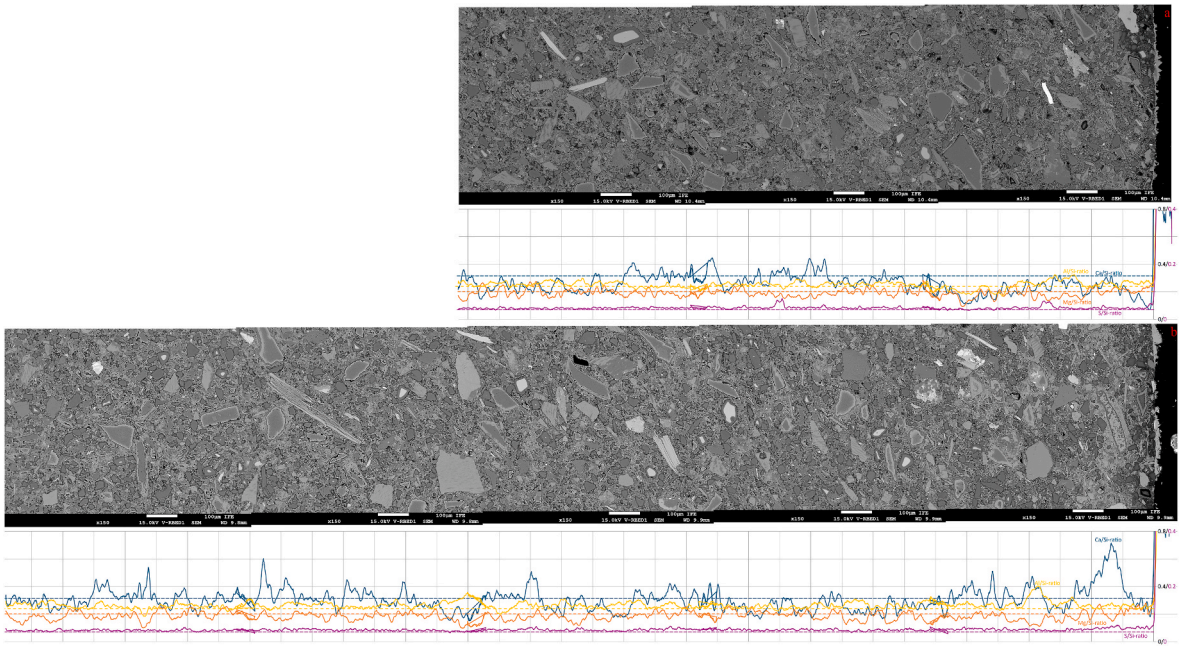

Fig. 22. SEM Micrographs of S5 samples exposed to wet supercritical CO_2 with 1.6 mol% H_2S for 4 (a) and 16 (b) weeks. The graphs underneath each micrograph show the Ca/Si, Mg/Si and Al/Si (blue, orange and yellow, respectively, all on the 0–0.8 axis), and S/Si (purple, on the 0–0.4 axis) elemental ratios (atom %/atom %) measured along the micrograph using EDS. The dashed lines are reference values (average values) measured at the centre of an unexposed sample. Scalebars shown with the micrographs and gridline spacing for the graphs are 100 μm.

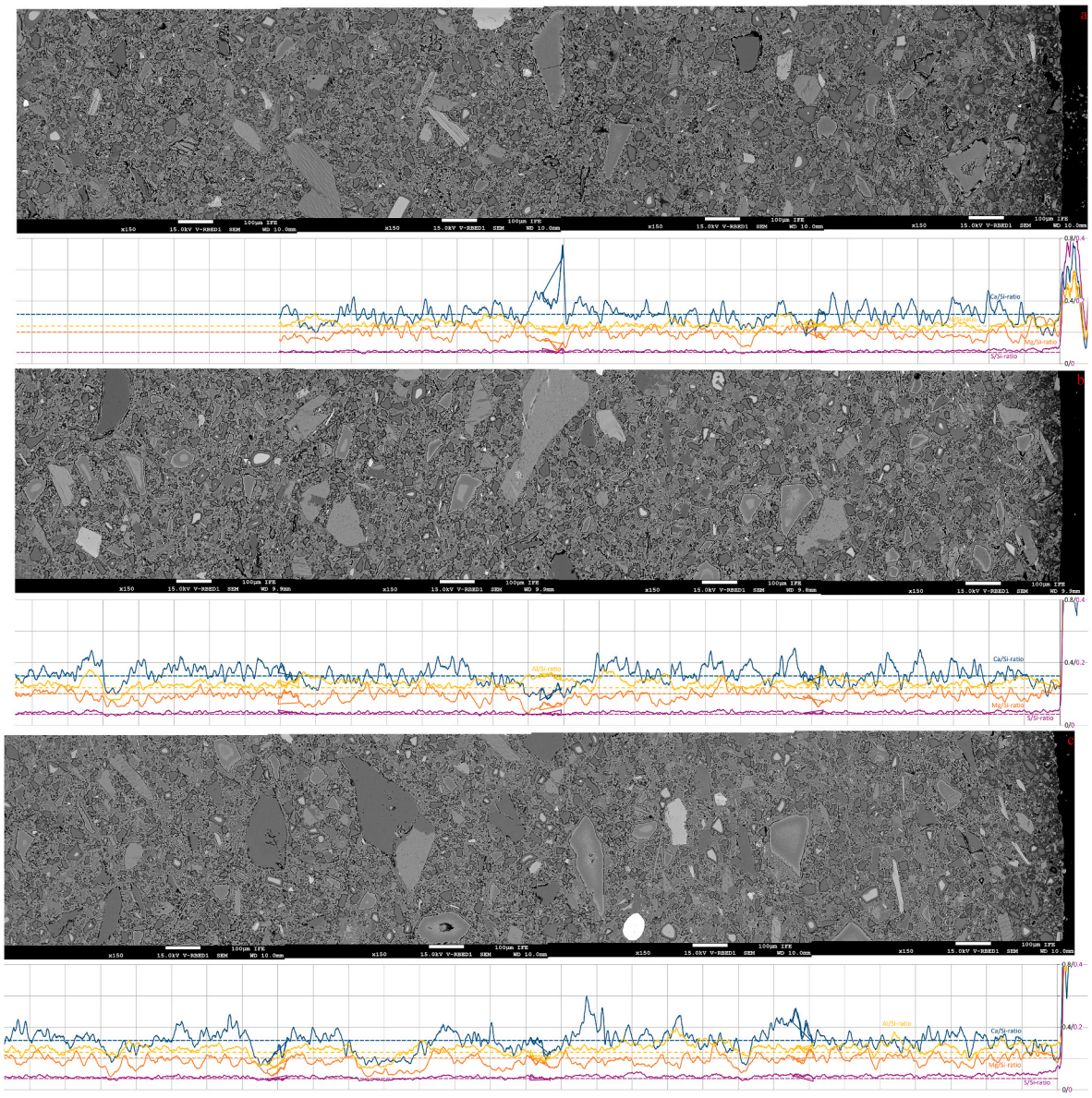

Fig. 23. SEM Micrographs of S5 samples exposed to wet supercritical CO_2 equilibrated with concentrated H_2SO_4 for 4 (a), 8 (b), and 16 (c) weeks. The graphs underneath each micrograph show the Ca/Si, Mg/Si and Al/Si (blue, orange and yellow, respectively, all on the 0–0.8 axis), and S/Si (purple, on the 0–0.4 axis) elemental ratios (atom %/atom %) measured along the micrograph using EDS. The dashed lines are reference values (average values) measured at the centre of an unexposed sample. Scalebars shown with the micrographs and gridline spacing for the graphs are 100 μm.

with H_2SO_4 was less altered near the sample surface. Whereas exposure to clean CO_2 or CO_2 with H_2S lead to densification due to enhanced carbonate precipitation in clearly delimited, relatively narrow outer zones, the sample exposed with H_2SO_4 only shows a feint, diffuse densification, similar to the S1-S3 samples exposed to CO_2 with H_2SO_4. SEM observations indicate some degradation at the sample surface, resulting in a reduction in matrix density and minor decrease in Ca/Si-ratio, but otherwise support the observed diffuse carbonation. While, based on sample mass changes, the S5 sample did not dry out during exposure, drying out of the outer shell can explain the relative lack of carbonation there, as well as more diffuse carbonation inwards. However, as for the PC-based sealants, acidification due to the presence of H_2SO_4 provides an alternative explanation for the lack of carbonate precipitation in the outer parts of these samples.

Finally, the negligible alterations induced by CO_2-exposure on S4 were not impacted by the presence of H_2SO_4. The sample mass decrease measured after 16 weeks exposure is close to the total water content as measured by drying a sample.

Considering the penetration of sulphate into the samples exposed to CO_2 with H_2SO_4, S/Si-ratios (or S/Al-ratios) are somewhat elevated in all samples. In the PC-based sealants (S1-S3), S/Si-ratios are consistently elevated throughout all exposed samples, though less elevated than in the samples exposed to wet supercritical CO_2 with H_2S. Furthermore, while in S1 the S/Si-ratio is elevated independently of distance to the surface, in S2 and S3, after 16 weeks exposure, it is somewhat more elevated in the outer 1300 and 2200 μm, respectively.

In S5, the S/Si-ratio is elevated throughout the sample, though most notably so in the outer ~300 μm. These elevated S/Si-ratios are comparably elevated to those observed in the S5 samples exposed to wet supercritical CO_2 with H_2S. Finally, while the presence of H_2SO_4 had negligible impact on the CO_2-exposure of S4, the S/Al-ratios are somewhat elevated in the outer 700–1000 μm of the exposed S4 samples, to comparable values as observed in the S4 samples exposed to wet supercritical CO_2 with H_2S.

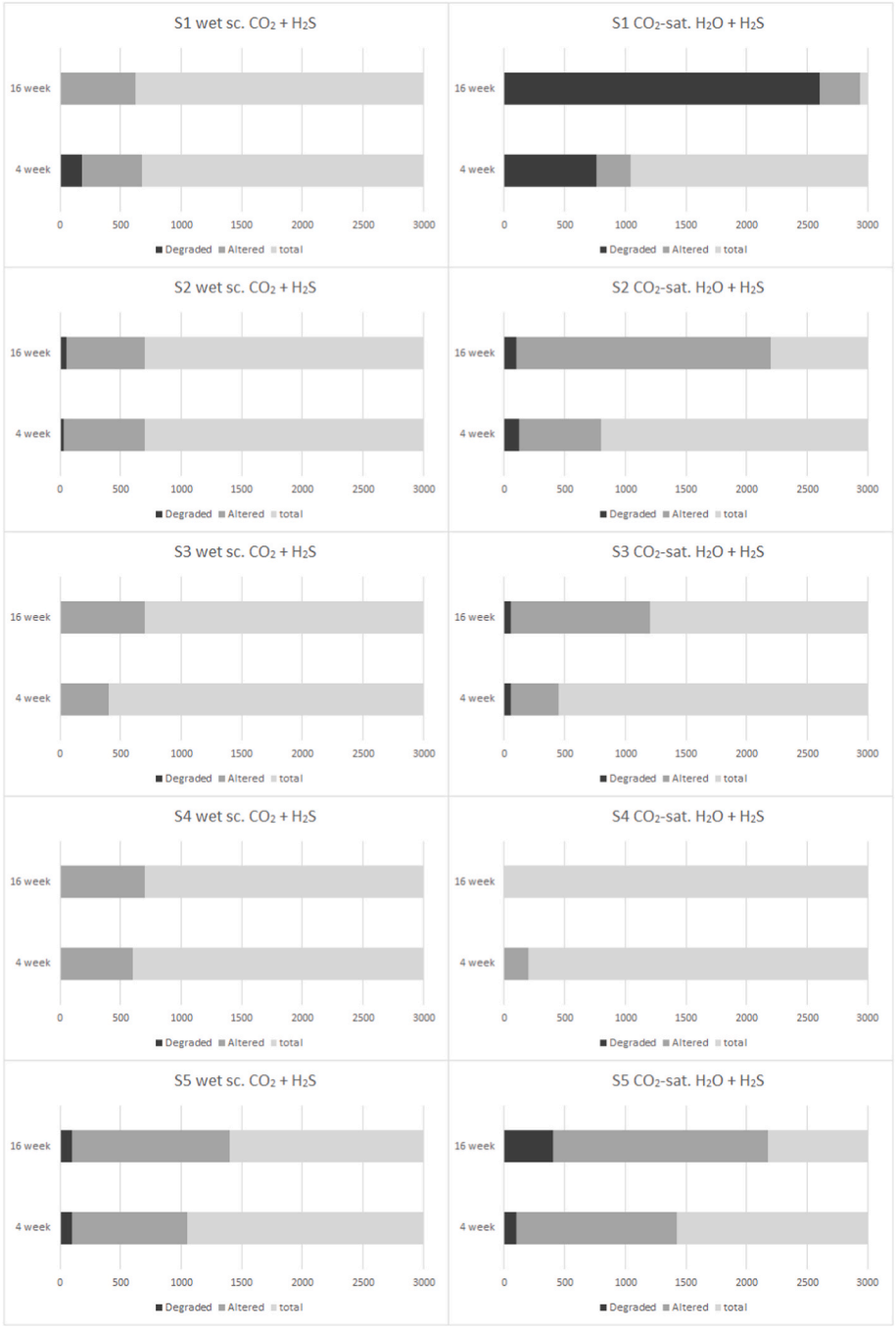

Fig. 24. Bar diagrams indicating the depths of degradation and the depth to which sealants were altered by exposure to CO_2 with H_2S based on SEM micrographs, elemental ratios, and CT scanning. "Degraded" indicates the depth to which the material is visibly degraded after exposure to CO_2 with H_2S, with elevated porosity, lowered mechanical competence, and (commonly) strongly altered chemical composition (e.g., Ca/Si-ratio). "Altered" indicates the depth from which the material appears unaltered, based on microstructure and assessed elemental ratios, though it should be noted that free $Ca(OH)_2$ in all samples was fully reacted already within 4 weeks exposure (see also (van Noort et al., 2025)).

4.4. Comparative analysis of the impact of impurities

In this study, five different sealants were exposed to CO_2 containing either H_2S or H_2SO_4, in the presence of water, at 80 °C and 10 MPa. For the former, samples were exposed to a water-saturated CO_2-phase containing 1.6 mol% H_2S, and a CO_2-saturated aqueous phase in equilibrium with that CO_2-phase, containing 0.087 mol% H_2S. While the H_2S concentration is much higher than what would be expected during GCS (cf. (NorthernLights, 2024)), it is well within the range found in existing reservoirs. For the latter, samples were exposed to a CO_2-phase in equilibrium with concentrated sulphuric acid, which could be considered a worst-case scenario for GCS. The impact of exposure was interpreted in terms of carbonation, alteration and degradation, and compared to previous experiments exposing the same five sealants to clean CO_2, at the same temperature and pressure. While exposure to CO_2-saturated water is commonly used to assess the resistance of sealants (or similar materials) to CO_2, during GCS in aquifers or depleted hydrocarbon reservoirs, the injected CO_2 will displace any water around the injection well, meaning exposure to (wet) supercritical CO_2 will be more relevant to the sealants in this well. In addition, as most reactive

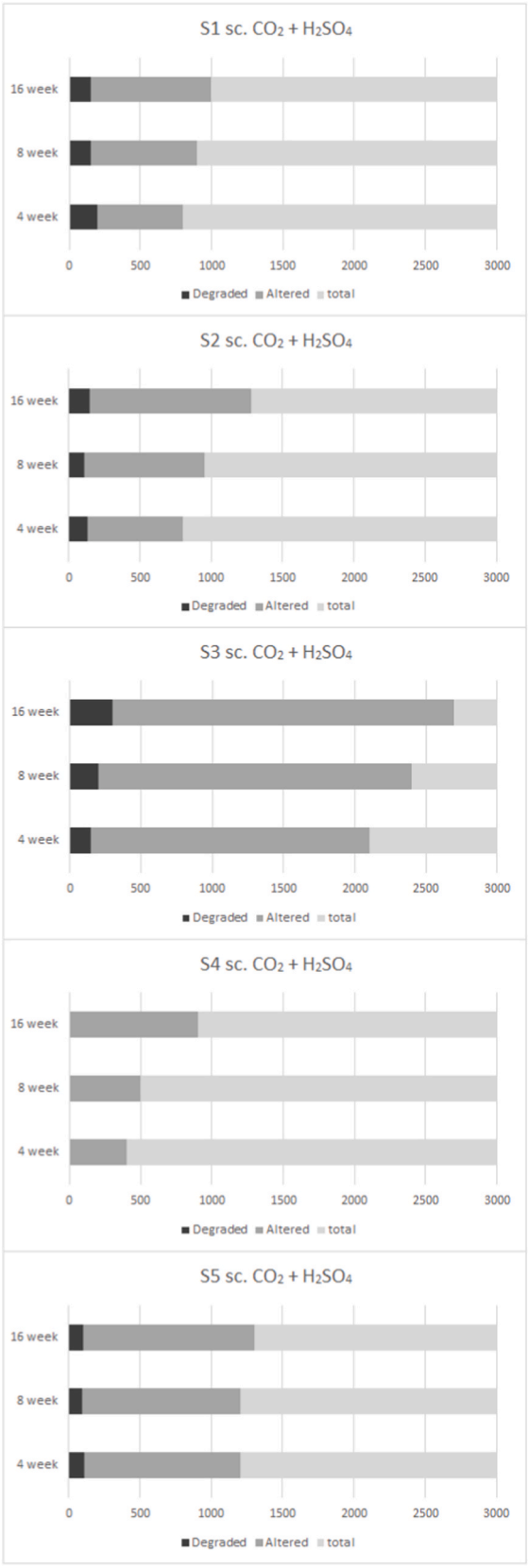

Fig. 25. Bar diagrams indicating the depths of degradation and the depth to which sealants were altered by exposure to CO_2 with H_2SO_4 based on SEM micrographs, elemental ratios, and CT scanning.

Table 4
Estimated sample water loss (as percentage of initial sample mass) after exposure to wet supercritical CO_2 with H_2SO_4, compared to samples exposed to clean wet supercritical CO_2.

Sealant	Estimated water loss after 4 weeks (wt.%)	Estimated water loss after 8 weeks (wt.%)	Estimated water loss after 16 weeks (wt.%)
S1	8.8 %	10.2 %	8.4 %
S2	8.3 %	9.5 %	10.7 %
S3	13.6 %	13.6 %	15.2 %
S4	7.5 %	16.0 %	18.1 %
S5	10.2 %	10.5 %	13.7 %

impurities are expected to remain in the near-wellbore area due to their strong partitioning into the water phase (Bachu and Bennion, 2009; Talman, 2015; Wolf et al., 2017; Xu et al., 2007), wells further away from the injection point are unlikely to be exposed significantly to these impurities. Therefore, in the following comparison of the impact of impurities on sealant integrity, only direct exposure to a CO_2-phase will be considered. Furthermore, as in the analyses performed here, sealant S4 was not affected significantly by exposure to CO_2, with or without the tested impurities, this will also be left out of the following discussion.

Based on testing with phenolphthalein (van Noort et al., 2025), all PC-based samples (sealants S1-S3) were fully carbonated within 4 weeks. However, while this meant that all free $Ca(OH)_2$ had reacted to $CaCO_3$, the sealants were otherwise not strongly affected in terms of their overall chemical composition or microstructural integrity. These properties were affected by subsequent alteration and degradation reaction fronts penetrating more slowly into the exposed samples. In PC-based samples S1-S3, the full penetration of carbonation corresponded to S/Si-ratios that were elevated from edge to core for all exposure durations, and for both H_2S and H_2SO_4. While these S/Si-ratios were ~1.5–2 times higher after H_2S-exposure, the S-content in the CO_2-phase with H_2S was also several order of magnitude higher, which could easily account for this difference. Microstructurally, in S1, exposure to H_2SO_4 led to a less dense microstructure in the outer zone compared to clean CO_2 or CO_2 with H_2S, due to a lower degree of carbonates precipitation. S2 shows similar trends, but in addition, from 100 to 150 μm from the sample edge, the carbonates precipitated with H_2SO_4 are much finer grained than for other exposure conditions, while in the outer 100–150 μm, carbonates are more similar in grain size to those observed in samples exposed to clean CO_2 or CO_2 with H_2S. In sealant S3, the presence of H_2SO_4 likewise resulted in the precipitation of finer-grained carbonates. Furthermore, as seen in the SEM images, in the PC-based sealants, exposure to CO_2 with H_2SO_4 led to degradation and reduced Ca/Si-ratios in an outer zone of up to 300 μm wide (though typically in the range 100–200 μm), whereas during exposure to wet supercritical CO_2 with H_2S degradation was only observed in some samples, and typically no deeper than ~50 μm. Likewise, for all three PC-based sealants, alteration depths were greater in the presence of H_2SO_4 than with H_2S or clean CO_2.

The presence of H_2S or H_2SO_4 during exposure to supercritical CO_2 had similar impacts on S5 as on the PC-based samples. In the presence of H_2S, enhanced precipitation of carbonates was restricted to a narrow outer zone between ~100 and ~250 μm from the sample surface. However, alteration (in particular a depletion of the Ca/Si-ratio) penetrated more deeply into the sample than with clean CO_2 (1400 vs. 960 μm). On the other hand, H_2SO_4 resulted in more disperse densification (due to enhanced carbonate precipitation), with densities being less elevated, but to greater depth – correlating with a more porous carbonate precipitate matrix observed in the SEM images. Alteration and degradation depths with H_2S and H_2SO_4 were similar, and higher than with clean CO_2, though for most sealants tested the increases were limited.

Overall, the above comparison shows that, even though the H_2SO_4 concentrations in the CO_2-phase were very low (0.091×10^{-3} mol%), the presence of H_2SO_4 had a clear impact on the microstructures of

exposed sealants, and was more deleterious overall than H_2S (at much higher concentration). Most notably, the presence of H_2SO_4 caused (minor) degradation at the surfaces of nearly all samples exposed (to a depth of ~100–200 μm), while such degradation was less common for exposure to wet supercritical CO_2 using either clean CO_2 or CO_2 with H_2S.

Large differences in exposed sample colour were observed between samples exposed to CO_2 with H_2S compared to samples exposed to clean CO_2 or CO_2 with H_2SO_4, where the former resulted in darker, blueish grey colours. This was ascribed to differences in oxidation state, and the formation of Fe-sulphides. XRD analysis should be included in a future study to confirm this interpretation, and to identify in what mineral species sulphur is bound within the sealants.

In this study, the impacts of only two impurities on sealant integrity were considered. The first impurity, H_2S, was selected as this impurity is common in natural reservoirs, and expected to be common in captured CO_2 as well. The second impurity, SO_x, added here in the form of H_2SO_4, was selected as this was identified as the impurity with the strongest potential impact on sealant integrity. Other key impurities that are expected to be reactive with typical sealant materials include NO_x (when reacting to form HNO_3), HCl and HF, which are all expected to cause acidification close to the injection point (cf. (Talman, 2015)), similar to SO_x. As nitrate and chloride salts are typically highly soluble, no additional effects of these impurities are expected, though the presence of NO_x could lead to oxidation, for example of ferrous iron to ferric iron. On the other hand, while HF is a weaker acid, the presence of F^- can lead to enhanced dissolution of silica through the formation of silica-fluoride complexes, and to the precipitation of insoluble phases such as CaF_2. As the enhanced dissolution of silica could lead to significant degradation, in projects where higher concentrations of HF may be expected, this potential impact should be studied experimentally.

4.5. Implications for sealant integrity

For all sealants tested, exposure to a CO_2-phase containing 1.6 mol% H_2S or to CO_2 equilibrated with concentrated H_2SO_4 did not change the main mechanisms by which CO_2-exposure lead to carbonation, alteration and degradation. However, especially for sealants based on PC, these impurities did impact the degrees to which these samples were affected by the different reactions that take place when they are exposed to CO_2, both in terms of depth and intensity.

Based on sample mass and fluid composition analyses, when sealants are exposed to CO_2-saturated water, the presence of H_2S can shift the balance between precipitation and dissolution of carbonates, leading to reduced overall carbonate precipitation. This was most apparent for the reference sealant, S1, which was also the most affected by clean CO_2, and this was further supported by microstructural evidence showing less carbonate precipitation and increased leaching in the S1 samples exposed to CO_2-saturated water with H_2S. In addition, the presence of H_2S, potentially as a consequence of the reduction in precipitated carbonates, increased the depth to which the sample was affected by about 1.5x. While in the other PC-based sealants, S2 and S3, higher concentrations of Mg were measured after 16 weeks of exposure to CO_2 with H_2S, mass measurements indicate somewhat stronger increases in mass after exposure compared to clean CO_2 for both these samples, while microstructural observations indicate somewhat deeper (1.2x in the case of S2) alteration, or enhanced intensity of alteration but with reduced alteration depths (S3). While microstructural evidence suggests that exposure of sealant S5 to CO_2-saturated water with H_2S lead to somewhat enhanced degradation, this is not supported by differences in sample mass after exposure, or by fluid composition. Sealant S4, which was non-reactive with CO_2, shows little impact of H_2S as well. Based on chemical analyses (expressed as S/Si-ratios), H_2S and CO_2 did fully penetrate the PC-based sealants (S1-S3), leading to the precipitation of submicron-sized particles of iron sulphide. In contrast, in sealant S4 elevated sulphur contents are mostly limited to the outer ~700 μm of exposed samples. In S5, S/Si-ratios were elevated throughout the samples, but less so than in samples S1-S3. Specific sulphide precipitates were not identified in S4 or S5, and more detailed study to identify such phases, using, for example, higher resolution SEM imaging, or XRD analysis should be considered in future work. Overall, when the sealants tested here were exposed to CO_2-saturated water at 80 °C and 10 MPa for up to 16 weeks, the presence of up to 1.6 mol% H_2S resulted in a limited enhancement of the alteration and degradation of the exposed sealants.

Considering exposure to (wet) supercritical CO_2, the impact of H_2S is again dependent on the sealant composition, but overall minor. While exposure of S2 to supercritical CO_2 with H_2S led to a somewhat smaller increase in mass, correlated with a more diffuse (deeper but less intense) densification zone in the CT-scans, other samples show no difference in mass change.

On the other hand, exposure to supercritical CO_2 with H_2SO_4 did lead to large decreases in sample mass compared to samples exposed to clean supercritical CO_2. However, this was ascribed to a drying out effect (experimental artefact), as water evaporated from the sealant samples to then be absorbed by the concentrated H_2SO_4 solution. Considering microstructural changes, this effect is associated with a more diffuse but deeper penetration of the densification caused by carbonate precipitation, such that microstructures are affected to depths 1.3 to 2 times greater than with clean CO_2. This deeper impact is interpreted as a result of the drying out of these samples rather than the presence of H_2SO_4 itself, as CO_2 has a higher mobility through the dried-out pore network, and can also travel more deeply through this pore network before dissolving into a hydrous pore fluid (and then precipitating as carbonate). However, a potential inhibition of carbonate precipitation due to an acidification effect cannot be excluded. While elevated S/Si-ratios in these samples do indicate a deeper penetration of sulphur, specific sulphate minerals (or other sulphur-binding minerals) were not identified, and a more detailed analysis needs to be performed in future work. The observed degradation in the outer ~100–200 μm of all samples exposed to H_2SO_4 (except S4) can be explained by the precipitation of droplets of highly acidic H_2SO_4 solution on the outer surface of the exposed samples, where H_2SO_4-saturated CO_2 encountered either liquid water, or wet CO_2 from inside the pore network. As these droplets grew in size, they then rained down from the samples, removing dissolved components. A rain of acid containing solutes from the exposed cements would also explain the colour changes observed in some of the H_2SO_4 vials placed underneath the samples. However, it cannot be fully excluded that sample degradation at the surface was caused by, for example, splashing with saturated H_2SO_4 solution during experiment start-up.

The experiments reported here thus show that the presence of relatively low concentrations of H_2S or H_2SO_4 in CO_2 in general resulted in mostly minor enhancement of the alteration and degradation of these materials compared to clean CO_2. One key impact of both impurities was a reduction in the quantity of precipitated carbonates in the outer parts of exposed samples. It should be noted that the H_2S content used here was much higher than expected during normal GCS (NorthernLights, 2024), but well within the range expected for, for example, EOR/EGR in sour fields. However, the impacts observed were more pronounced on sealants that were also more affected by CO_2. This suggests that these impacts are also more enhanced under exposure conditions where sealants are more strongly affected by CO_2, such as under conditions where CO_2 leaks along a crack through a cement-based seal, or along an annular gap. Under such conditions, the presence of reactive impurities such as H_2S or H_2SO_4 may lead to a deeper and more intense alteration of the leakage pathway side-wall, which may exacerbate the leak. Inhibition of carbonate precipitation, such as was observed in the experiments reported here, may also limit self-sealing effects that would otherwise reduce the aperture and stop leakage.

While the impacts of impurities observed here were relatively limited, further research on the impact of impurities on wellbore sealant integrity when exposed to CO_2 is warranted. As the effect of impurities is correlated to sealant composition, studies on a wider range of sealant

compositions should map whether other sealants (for example with lower SiO_2-content) are impacted more strongly. Likewise, the impact of other relatively reactive impurities, such as NO_x or HF, as well as key combinations of impurities should be assessed in laboratory experiments. Temperature and pressure-dependencies should likewise be addressed. As impurities could have a more pronounced impact on the evolution of leakage pathways once a such a pathway has been established, this should also be assessed directly, for example through experiments simulating the flow of CO_2 with impurities along a leakage pathway under in-situ conditions.

Finally, as a drying out zone is expected to form around an injection wellbore used to inject CO_2 (Bachu, 2000; Miri et al., 2015; Peysson et al., 2014; Pruess and Müller, 2009), the interplay between drying out and carbonation (similar to that seen in the H_2SO_4-experiments reported here) also needs to be considered in more detail, through further experimental study.

5. Summary and conclusions

In the experimental research reported here, five different wellbore sealants (S1 – S5) were exposed to CO_2 with H_2S or H_2SO_4 at 80 °C and 10 MPa for up to 16 weeks. These experiments were carried out to assess how these key impurities impact wellbore seal integrity during CO_2-injection and -storage in geological reservoirs. Microstructural and chemical analyses of the exposed sealant samples and exposure fluids showed that, in general, exposure to CO_2-saturated water led to carbonate precipitation, as well as some material degradation through the leaching of soluble ions (such as Ca and Mg), while direct exposure to a (wet) supercritical CO_2-phase mostly resulted in density enhancement through carbonate precipitation in the outer areas of the exposed samples. Based on the results obtained, it can be concluded that.

- During exposure to CO_2-saturated water, in most sealants tested the presence of H_2S enhanced the alterations observed. This resulted in deeper alteration depths (such as depletion of the Ca/Si-ratio) in sealants S1, S2 and S5. In sealants S1 and S5, the presence of H_2S also inhibited carbonate precipitation, and enhanced material degradation. The impact of H_2S was less pronounced on sealants that were less reactive with CO_2 (especially S4).
- During exposure to wet supercritical CO_2, the presence of H_2S had a limited impact on alteration and degradation, mainly leading to deeper microstructural alteration in sealants S1 and S5. The presence of H_2S also resulted in less densification due to carbonate precipitation in the outer parts of exposed samples.
- During exposure to supercritical CO_2 with H_2SO_4, sample alterations were affected by both the presence of H_2SO_4, and the observed desiccation of the samples due to the absorption of water by the concentrated sulphuric acid (i.e., an experimental artefact). Mainly, microstructural densification due to carbonate precipitation in the presence of H_2SO_4 was more diffuse, causing up to 2 times higher alteration depths in these samples. This may be partly ascribed to desiccation resulting in deeper CO_2-penetration before mineralisation as the CO_2-water interface receded, or alternatively to the acidifying effect of H_2SO_4. In addition, samples exposed to CO_2 with H_2SO_4 also showed more degradation at the surfaces, though this was mostly limited to the outer 100–200 μm of these samples (and the degree of this degradation was quite minor). This degradation may be the result of the formation and subsequent run-off of highly acidic liquid droplets at the sample surfaces, where H_2SO_4-saturated CO_2 encountered water and precipitated.
- For geological CO_2-storage applications, the impact of impurities co-injected with CO_2 on intact seals with compositions similar to those tested here, and under similar PT-conditions, will likely be relatively minor, at worst leading to an increase in alteration depths by (considerably) less than an order of magnitude.
- When CO_2 (or CO_2-saturated water) flows along a leakage pathway through or along a wellbore seal, however, reactive impurities in the CO_2 may impact how this leakage pathway develops, potentially exacerbating the leakage, for example by inhibiting carbonate precipitation that could otherwise lead to self-sealing of the leakage pathway.
- More work is needed, to assess a wider range of sealant compositions, and to address the impact of other reactive impurities (and combinations of impurities) than those studied here (e.g., NO_x, O_2 and HF). The impact of impurities on leakage pathway development also needs to be studied in more detail in targeted laboratory experiments, to constrain this potential storage integrity risk.

Funding statement

The CEMENTEGRITY project is funded through the ACT programme (Accelerating CCS Technologies, Horizon2020 Project No 691712). Financial contributions from the Research Council of Norway (RCN), the Netherlands Enterprise Agency (RVO), the Department for Energy Security & Net Zero (DESNZ, UK), and Harbour Energy are gratefully acknowledged.

CRediT authorship contribution statement

Reinier van Noort: Writing – original draft, Visualization, Supervision, Project administration, Methodology, Investigation, Funding acquisition, Formal analysis, Conceptualization. **Gaute Svenningsen:** Writing – review & editing, Methodology, Investigation, Funding acquisition. **Kai Li:** Resources, Investigation.

Declaration of competing interest

The authors declare the following financial interests/personal relationships which may be considered as potential competing interests: Reinier van Noort reports financial support was provided by Harbour Energy. Reinier van Noort reports samples were provided by Halliburton. If there are other authors, they declare that they have no known competing financial interests or personal relationships that could have appeared to influence the work reported in this paper.

Data availability

Data will be made available on request.

References

Abid, K., Gholami, R., Choate, P., Nagaratnam, B.H., 2015. A review on cement degradation under CO2-rich environment of sequestration projects. J. Nat. Gas Sci. Eng. 27, 1149–1157. https://doi.org/10.1016/j.jngse.2015.09.061.

API, 2013. Recommended Practice 10B-2: Recommended Practice for Testing Well Cements. American Petroleum Institute.

Bachu, S., 2000. Sequestration of CO2 in geological media: criteria and approach for site selection in response to climate change. Energy Convers. Manag. 41 (9), 953–970. https://doi.org/10.1016/S0196-8904(99)00149-1.

Bachu, S., Bennion, D.B., 2009. Chromatographic partitioning of impurities contained in a CO2 stream injected into a deep saline aquifer: part 1. Effects of gas composition and in situ conditions. Int. J. Greenh. Gas Control 3 (4), 458–467. https://doi.org/10.1016/j.ijggc.2009.01.001.

Barlet-Gouédard, V., Rimmelé, G., Goffé, B., Porcherie, O., 2006. Mitigation strategies for the risk of CO2 migration through wellbores. In: IADC/SPE Drilling Conference. https://doi.org/10.2118/98924-MS. Miami, Florida, USA.

Bjørge, R., Gawel, K., Chavez Panduro, E.A., Torsæter, M., 2019. Carbonation of silica cement at high-temperature well conditions. Int. J. Greenh. Gas Control 82, 261–268. https://doi.org/10.1016/j.ijggc.2019.01.011.

Brunet, J.-P.L., Li, L., Karpyn, Z.T., Kutchko, B.G., Strazisar, B., Bromhal, G., 2013. Dynamic evolution of cement composition and transport properties under conditions relevant to geological carbon sequestration. Energy Fuel. 27 (8), 4208–4220. https://doi.org/10.1021/ef302023v.

Carey, J.W., Wigand, M., Chipera, S.J., WoldeGabriel, G., Pawar, R., Lichtner, P.C., Wehner, S.C., Raines, M.A., Guthrie, G.D., 2007. Analysis and performance of oil well cement with 30 years of CO2 exposure from the SACROC unit, west Texas, USA.

Int. J. Greenh. Gas Control 1 (1), 75–85. https://doi.org/10.1016/S1750-5836(06)00004-1.
Chavez Panduro, E.A., Torsæter, M., Gawel, K., Bjørge, R., Gibaud, A., Yang, Y., Bruns, S., Zheng, Y., Sørensen, H.O., Breiby, D.W., 2017. In-Situ X-ray tomography study of cement exposed to CO(2) saturated brine. Environ. Sci. Technol. 51 (16), 9344–9351. https://doi.org/10.1021/acs.est.6b06534.
Crow, W., Brian Williams, D., William Carey, J., Celia, M., Gasda, S., 2009. Wellbore integrity analysis of a natural CO2 producer. Energy Proc. 1 (1), 3561–3569. https://doi.org/10.1016/j.egypro.2009.02.150.
Duguid, A., 2009. An estimate of the time to degrade the cement sheath in a well exposed to carbonated brine. Energy Proc. 1 (1), 3181–3188. https://doi.org/10.1016/j.egypro.2009.02.101.
Duguid, A., Scherer, G.W., 2010. Degradation of oilwell cement due to exposure to carbonated brine. Int. J. Greenh. Gas Control 4 (3), 546–560. https://doi.org/10.1016/j.ijggc.2009.11.001.
Equinor, 2019. *Northern Lights Project Concept report* (RE-PM673-00001). https://ccsnorway.com/app/uploads/sites/6/2020/05/Northern-Lights-Project-Concept-report.pdf.
Gu, T., Guo, X., Li, Z., Cheng, X., Fan, X., Korayem, A., Duan, W.H., 2017. Coupled effect of CO2 attack and tensile stress on well cement under CO2 storage conditions. Constr. Build. Mater. 130, 92–102. https://doi.org/10.1016/j.conbuildmat.2016.10.117.
Hernández-Rodríguez, A., Montegrossi, G., Huet, B., Vaselli, O., Virgili, G., 2017. A study of wellbore cement alteration controlled by CO2 leakage in a natural analogue for geological CO2 storage. Appl. Geochem. 86, 13–25. https://doi.org/10.1016/j.apgeochem.2017.09.010.
Jacquemet, N., Pironon, J., Lagneau, V., Saint-Marc, J., 2012. Armouring of well cement in H2S–CO2 saturated brine by calcite coating – experiments and numerical modelling. Appl. Geochem. 27 (3), 782–795. https://doi.org/10.1016/j.apgeochem.2011.12.004.
Jacquemet, N., Pironon, J., Saint-Marc, J., 2008. Mineralogical changes of a well cement in various H2S-CO2(-Brine) fluids at high pressure and temperature. Environ. Sci. Technol. 42 (1), 282–288. https://doi.org/10.1021/es070853s.
Kutchko, B., Lopano, C., Strazisar, B., Hawthorne, S., Miller, D., Thaulow, N., Zhang, L., Guthrie, G., 2015. Impact of oil well cement exposed to H2S saturated fluid and gas at high temperatures and pressures: implications for acid gas injection and Co-Sequestration. J. Sustainable Energy Eng. 3 (1), 80–101. https://doi.org/10.7569/jsee.2015.629509.
Kutchko, B.G., Strazisar, B.R., Dzombak, D.A., Lowry, G.V., Thaulow, N., 2007. Degradation of well cement by CO2 under geologic sequestration conditions. Environ. Sci. Technol. 41 (13), 4787–4792. https://doi.org/10.1021/es062828c.
Kutchko, B.G., Strazisar, B.R., Hawthorne, S.B., Lopano, C.L., Miller, D.J., Hakala, J.A., Guthrie, G.D., 2011. H2S–CO2 reaction with hydrated class H well cement: acid-gas injection and CO2 Co-sequestration. Int. J. Greenh. Gas Control 5 (4), 880–888. https://doi.org/10.1016/j.ijggc.2011.02.008.
Kutchko, B.G., Strazisar, B.R., Huerta, N., Lowry, G.V., Dzombak, D.A., Thaulow, N., 2009. CO2 reaction with hydrated class H well cement under geologic sequestration conditions: effects of flyash admixtures. Environ. Sci. Technol. 43 (10), 3947–3952. https://doi.org/10.1021/es803007e.
Kutchko, B.G., Strazisar, B.R., Lowry, G.V., Dzombak, D.A., Thaulow, N., 2008. Rate of CO2 attack on hydrated class H well cement under geologic sequestration conditions. Environ. Sci. Technol. 42 (16), 6237–6242. https://doi.org/10.1021/es800049r.
Laudet, J.-B., Garnier, A., Neuville, N., Le Guen, Y., Fourmaintraux, D., Rafai, N., Burlion, N., Shao, J.-F., 2011. The behavior of oil well cement at downhole CO2 storage conditions: static and dynamic laboratory experiments. Energy Proc. 4, 5251–5258. https://doi.org/10.1016/j.egypro.2011.02.504.
Lende, G., Clausen, J.A., Kvassnes, A.J., 2021. Evaluation of new innovative cement blend for enhanced CO2 and H2S resistance. In: SPE/IADC International Drilling Conference and Exhibition 2021. https://doi.org/10.2118/204103-MS.
Lende, G., Sørensen, E., Jandhyala, S.R.K., Van Noort, R., 2024. *State of the art test method to quantify progression rate of carbonation of wellbore sealing materials* SPE Europe energy conference and exhibition, Turin, Italy. https://doi.org/10.2118/220113-MS.
Lesti, M., Tiemeyer, C., Plank, J., 2013. CO2 stability of Portland cement based well cementing systems for use on carbon capture & storage (CCS) wells. Cement Concr. Res. 45, 45–54. https://doi.org/10.1016/j.cemconres.2012.12.001.
Liteanu, E., Spiers, C.J., 2011. Fracture healing and transport properties of wellbore cement in the presence of supercritical CO2. Chem. Geol. 281 (3), 195–210. https://doi.org/10.1016/j.chemgeo.2010.12.008.
Matteo, E.N., Scherer, G.W., 2012. Experimental study of the diffusion-controlled acid degradation of class H Portland cement. Int. J. Greenh. Gas Control 7, 181–191. https://doi.org/10.1016/j.ijggc.2011.07.012.
Miri, R., van Noort, R., Aagaard, P., Hellevang, H., 2015. New insights on the physics of salt precipitation during injection of CO2 into saline aquifers. Int. J. Greenh. Gas Control 43, 10–21. https://doi.org/10.1016/j.ijggc.2015.10.004.
Morland, B.H., Dugstad, A., Svenningsen, G., 2022. Experimental based CO2 transport specification ensuring material integrity. Int. J. Greenh. Gas Control 119, 103697. https://doi.org/10.1016/j.ijggc.2022.103697.
Morland, B.H., Tadesse, A., Svenningsen, G., Springer, R.D., Anderko, A., 2019a. Nitric and sulfuric acid solubility in dense phase CO2. Ind. Eng. Chem. Res. https://doi.org/10.1021/acs.iecr.9b04957.
Morland, B.H., Tjelta, M., Norby, T., Svenningsen, G., 2019b. Acid reactions in hub systems consisting of separate non-reactive CO2 transport lines. Int. J. Greenh. Gas Control 87, 246–255. https://doi.org/10.1016/j.ijggc.2019.05.017.
NorthernLights, 2024. *Liquid CO2 quality specifications for the Northern Lights* (NL-02-TE-SP01 rev 1). https://norlights.com/wp-content/uploads/2024/06/NorthernLights-GS-co2-spec2024.pdf.
Omosebi, O., Maheshwari, H., Ahmed, R., Shah, S., Osisanya, S., Santra, A., Saasen, A., 2015. Investigating temperature effect on degradation of well cement in HPHT carbonic acid environment. J. Nat. Gas Sci. Eng. 26, 1344–1362. https://doi.org/10.1016/j.jngse.2015.08.018.
Peysson, Y., André, L., Azaroual, M., 2014. Well injectivity during CO2 storage operations in deep saline aquifers—Part 1: experimental investigation of drying effects, salt precipitation and capillary forces. Int. J. Greenh. Gas Control 22, 291–300. https://doi.org/10.1016/j.ijggc.2013.10.031.
Pruess, K., Müller, N., 2009. Formation dry-out from CO2 injection into saline aquifers: 1. Effects of solids precipitation and their mitigation. Water Resour. Res. 45 (3). https://doi.org/10.1029/2008WR007101.
Sterpenich, J., Jobard, E., El Hajj, H., Pironon, J., Randi, A., Caumon, M.-C., 2014. Experimental study of CO2 injection in a simulated injection well: the MIRAGES experiment. Greenhouse Gas.: Sci. Technol. 4 (2), 210–224. https://doi.org/10.1002/ghg.1389.
Talman, S., 2015. Subsurface geochemical fate and effects of impurities contained in a CO2 stream injected into a deep saline aquifer: what is known. Int. J. Greenh. Gas Control 40, 267–291. https://doi.org/10.1016/j.ijggc.2015.04.019.
Todorovic, J., Lange, T., Stroisz, A.M., Duda, M., Agofack, N., Nilsen, N.I., 2023. *Barrier Material Robustness Towards Corrosive Environment.* SWIPA Annual Conference 2023. Trondheim, 2023-03-30 - 2023-03-31. https://www.sintef.no/en/publications/publication/2143604/.
Todorovic, J., Opedal, N.V., Werner, B., Clausen, J.A., Kvassnes, A.J.S., 2020. Effect of long-term aging in carbonated brine on mechanical properties of a novel cement system with an expandable agent. In: SPE Norway Subsurface Conference.
van Noort, R., Svenningsen, G., Li, K., Pluymakers, A., 2025. Exposure of five cementitious sealant materials to wet supercritical CO2 and CO2-saturated water under simulated downhole conditions. Int. J. Greenh. Gas Control 144, 104380. https://doi.org/10.1016/j.ijggc.2025.104380.
Walsh, S.D.C., Mason, H.E., Du Frane, W.L., Carroll, S.A., 2014. Experimental calibration of a numerical model describing the alteration of cement/caprock interfaces by carbonated brine. Int. J. Greenh. Gas Control 22, 176–188. https://doi.org/10.1016/j.ijggc.2014.01.004.
Wigand, M., Kaszuba, J.P., Carey, J.W., Hollis, W.K., 2009. Geochemical effects of CO2 sequestration on fractured wellbore cement at the cement/caprock interface. Chem. Geol. 265 (1), 122–133. https://doi.org/10.1016/j.chemgeo.2009.04.008.
Wolf, J.L., Niemi, A., Bensabat, J., May, F., Rütters, H., Rebscher, D., 2017. 2D reactive transport simulations of CO2 streams containing impurities in a saline aquifer, Heletz, Israel. Energy Proc. 114, 3537–3546. https://doi.org/10.1016/j.egypro.2017.03.1483.
Xiao, T., McPherson, B., Bordelon, A., Viswanathan, H., Dai, Z., Tian, H., Esser, R., Jia, W., Carey, W., 2017. Quantification of CO2-cement-rock interactions at the well-caprock-reservoir interface and implications for geological CO2 storage. Int. J. Greenh. Gas Control 63, 126–140. https://doi.org/10.1016/j.ijggc.2017.05.009.
Xu, T., Apps, J.A., Pruess, K., Yamamoto, H., 2007. Numerical modeling of injection and mineral trapping of CO2 with H2S and SO2 in a sandstone formation. Chem. Geol. 242 (3), 319–346. https://doi.org/10.1016/j.chemgeo.2007.03.022.
Zhang, L., Dzombak, D.A., Nakles, D.V., Hawthorne, S.B., Miller, D.J., Kutchko, B., Lopano, C., Strazisar, B., 2014a. Effect of exposure environment on the interactions between acid gas (H2S and CO2) and pozzolan-amended wellbore cement under acid gas co-sequestration conditions. Int. J. Greenh. Gas Control 27, 309–318. https://doi.org/10.1016/j.ijggc.2014.06.030.
Zhang, L., Dzombak, D.A., Nakles, D.V., Hawthorne, S.B., Miller, D.J., Kutchko, B.G., Lopano, C.L., Strazisar, B.R., 2014b. Rate of H2S and CO2 attack on pozzolan-amended class H well cement under geologic sequestration conditions. Int. J. Greenh. Gas Control 27, 299–308. https://doi.org/10.1016/j.ijggc.2014.02.013.
Zhang, M., Talman, S., 2014. Experimental study of well cement carbonation under geological storage conditions. Energy Proc. 63, 5813–5821. https://doi.org/10.1016/j.egypro.2014.11.614.